

1 A Method for Objectively Integrating Soil Moisture Satellite Observations and
2 Model Simulations toward a Blended Drought Index

3 Jifu Yin^{1,2*}, Xiwu Zhan², Christopher R. Hain³, Jicheng Liu^{1,2}, Martha C. Anderson⁴

4 ¹ ESSIC/CICS, University of Maryland College Park, College Park 20740, MD, USA.

5 ² NOAA NESDIS Center for Satellite Applications and Research, College Park 20740, MD, USA.

6 ³ Marshall Space Flight Center, Earth Science Branch, Huntsville 35801, AL, USA

7 ⁴ USDA-ARS, Hydrology and Remote Sensing Laboratory, Beltsville 20704, MD, USA.

8

9 *Corresponding author: Dr. Jifu Yin, National Oceanic and Atmospheric Administration (NOAA)

10 NESDIS STAR/SMCD, 5830 University Research Court, College Park, MD 20740, USA. Email:

11 jifu.yin@noaa.gov

12

13

14

15

16

17

18 Abstract: With satellite soil moisture (SM) retrievals becoming widely and continuously
19 available, we aim to develop a method to objectively integrate the drought indices into one that is
20 more accurate and consistently reliable. The datasets used in this paper include the Noah land
21 surface model-based SM estimations, Atmosphere-Land-Exchange-Inverse model-based
22 Evaporative Stress Index, and the satellite SM products from the Advanced Scatterometer,
23 WindSat, Soil Moisture and Ocean Salinity, and Soil Moisture Operational Product System. Using
24 the Triple Collocation Error Model (TCEM) to quantify the uncertainties of these data, we
25 developed an optically blended drought index (BDI_b) that objectively integrates drought
26 estimations with the lowest TCEM-derived root-mean-square-errors in this paper. With respect to
27 the reported drought records and the drought monitoring benchmarks including the U.S. Drought
28 Monitor, the Palmer Drought Severity Index and the standardized precipitation evapotranspiration
29 index products, the BDI_b was compared with the sample average blending drought index (BDI_s)
30 and the RMSE-weighted average blending drought indices (BDI_w). Relative to the BDI_s and
31 the BDI_w, the BDI_b performs more consistently with the drought monitoring benchmarks. With
32 respect to the official drought records, the developed BDI_b shows the best performance on
33 tracking drought development in terms of time evolution and spatial patterns of 2010-Russia,
34 2011-USA, 2013-New Zealand droughts and other reported agricultural drought occurrences over
35 the 2009-2014 period. These results suggest that model simulations and remotely sensed
36 observations of SM can be objectively translated into useful information for drought monitoring
37 and early warning, in turn can reduce drought risk and impacts.

38 Keywords: Drought monitoring, Soil moisture, Triple collocation, Blended drought index

39

40 1. Introduction

41 Of all natural disasters, the economic and environmental consequences of drought are
42 among the most serious due to the duration varying from weeks to decades, and widespread spatial
43 extent (Lewis *et al.*, 2011; Mu *et al.*, 2013; Hao *et al.*, 2014; Anderson *et al.*, 2015; Mazdidasni
44 and AghaKouchak, 2015; AghaKouchak *et al.*, 2015; Zhang *et al.*, 2017). Associated with global
45 climate change, the frequency, duration and severity of drought events show an increasing
46 tendency in some parts of the world (Dai, 2013; Mazdidasni and AghaKouchak, 2015). Drought
47 indicator development is essential for monitoring drought conditions, providing timely seasonal
48 forecasts, and consequently reducing drought risk and impacts (Tarhule and Lamb 2003; Pozzi *et*
49 *al.* 2013; Sheffield *et al.*, 2014).

50 Agricultural drought is commonly defined as an event where root-zone soil moisture (SM)
51 deficits result in a reduction in crop yields, plant biomass and ecologic productivity (Wilhite and
52 Glantz 1985; Anderson *et al.*, 2011; Bolten and Crow, 2012; McNally *et al.*, 2015, Azmi *et al.*,
53 2016; Zhang *et al.*, 2017). The SM status in various soil layers is an important indicator of
54 agricultural drought, providing more information than the rainfall anomaly alone. Modern land
55 surface models (LSMs) offer a complex parameterization of the surface energy balance and
56 detailed vertical water balance physics in an attempt to more accurately characterize temporal
57 variations in root-zone soil moisture availability (Koster *et al.*, 2000; Yang *et al.*, 2003; Ek *et al.*,
58 2003; Dai *et al.*, 2003; Oleson *et al.*, 2004; Kowalczyk *et al.*, 2006; Crow *et al.*, 2012; Yin *et al.*,
59 2015a). However, these model-based estimates are typically subject to errors in the model physics
60 and parameterizations, and in the meteorological forcing data (Reichle and Koster, 2004; Yin *et*
61 *al.*, 2014; Yin *et al.*, 2015b). Data assimilation techniques permit the modelled soil moisture (SM)
62 to be corrected toward the observations with the correction degree determined by the error levels

63 associated with each (Reichle and Koster, 2004). With satellite SM retrievals becoming widely
64 and continuously available, it is consequently believed that a land data assimilation system that
65 merges satellite retrievals and model estimates of soil moisture may provide more reasonable
66 values of land surface state variables (Crow and Wood, 2003; Reichle and Koster, 2004; Koster *et*
67 *al.*, 2009; Kumar *et al.* 2009; Xia *et al.*, 2012; Hain *et al.* 2012; Zhan *et al.* 2012; Yin *et al.*, 2015b,
68 2015c). In the most widely used ensemble Kalman filter (EnKF), still, satellite SM observations
69 need to be bias-corrected to respect the assumption that retrieval errors are Gaussian-distributed.
70 The current bias-correction approaches used for the EnKF data assimilation might have caused
71 useful information in the observations lost in the model simulations (Nearing *et al.*, 2016).

72 While in situ measurements of SM provide reasonable assessments of moisture conditions
73 at the local scale, they are deficient in representing the soil moisture and drought dynamics at large
74 scales due to insufficient data coverage (Yuan *et al.*, 2015). In contrast, microwave (MW, active
75 or passive) remote sensing observations can provide spatially consistent estimates of the SM state.
76 Although they can only sense the surface soil depth, usually within 0-5 cm (Kerr *et al.*, 2001;
77 Njoku *et al.*, 2003; Naeimi *et al.*, 2009; Yin *et al.*, 2015b; Wang *et al.*, 2015), there is generally a
78 close relationship between surface SM and SM in the deeper soil layers at weekly and longer time
79 scale (Albergel *et al.*, 2008). The SM status in surface soil layer represents the fastest response soil
80 moisture dynamics to meteorological anomalies and provides a measure for short-term droughts
81 (Yuan *et al.*, 2015); and the surface information propagating to deeper soil layers is very important
82 to early warning agricultural droughts and monitoring flash droughts that can occur very rapidly
83 (Otkin *et al.*, 2015). However, the MW SM products suffer from the instrument noise and
84 uncertainty in microwave emission modeling. Land surface temperature (LST)- and green
85 vegetation fraction (GVF)-based quality control of the satellite SM retrievals can decrease the

86 impacts of these uncertainties, but the empirical approaches are hard to be widely used (Kumar *et*
87 *al.*, 2009; Yin *et al.*, 2014).

88 Comparison of MW SM products to ground-based SM observations is the most common error
89 estimation approach; however, the in situ observational data from low density networks in which
90 one or two measurements are generally available per satellite footprint can lead to significant
91 differences in the spatial sampling scale (Crow *et al.*, 2005; Koster *et al.*, 2009; Miralles *et al.*,
92 2010). A triple collocation error model (TCEM) methodology was introduced to estimate the root
93 mean square errors (RMSE) while simultaneously solving for systematic differences in the
94 climatologies of a set of three independent data sources (Scipal *et al.*, 2008; Miralles *et al.*, 2010;
95 Crow *et al.*, 2015; Pan *et al.*, 2015). Based on three separate time series assumed to approximate
96 grid-scale SM products, the TCEM in previous reports exhibited robust capability to assess novel
97 remotely sensed SM data sets in comparison with LSM estimations and in-situ observations in a
98 limited number of well sampled pixels (Miralles *et al.*, 2010; Draper *et al.*, 2013).

99 Drought monitoring is a complex and multi-faceted endeavor, warranting use of multiple
100 tools and indicators; the nature of drought monitoring efforts should thus be based on multiple
101 variables/indicators to provide a more robust and integrated measure of drought through a
102 convergence-of-evidence methodology (AghaKouchak *et al.*, 2015). Current operational drought
103 monitoring products (Svoboda *et al.*, 2002; Heim, 2002; Xia *et al.*, 2014) are generally produced
104 via integrating multiple data sources and derivative products based on a synthesis of
105 indicators/model-simulations and subjective interpretation of how different indicators/model-
106 simulations should be merged in the final analysis. These routinely running drought monitoring
107 products are thus sensitive to the experts' experiences/judgment and the model uncertainties from
108 errors in the indicators. These types of artificial and product errors can be compensated for by

109 objectively merging multi-sources drought evaluations through uncertainty-based optimization of
110 remotely sensed observations and model estimations.

111 Additionally, to capture different drought characteristic, numerous multivariate drought
112 indices have been recently proposed. The ordinal regression model permits to estimate the
113 probability of each drought category, and in turn to highlight probabilistic drought characterization
114 in the categorical form (Hao et al., 2016). Yet its properly implement is limited by optimal choice
115 of three drought indices in different regions and seasons. Besides, other blended drought indicators
116 including the principal component analysis-based multivariate Aggregate Drought Index
117 (Keyantash and Dracup, 2004; Rajsekhar et al., 2015), the joint distribution of the accumulated
118 precipitation and streamflow-based Joint Drought Index (Kao and Govindaraju, 2010) and
119 Multivariate Standardized Drought Index (Hao and AghaKouchak, 2013) are basically based on
120 the water balance model and multivariate analysis (Hao et al., 2015). Thus, development of a
121 method for objectively integrating soil moisture satellite observations and model simulations
122 toward a blended drought index is still challenging. This paper is an attempt in this direction

123 In this paper, we aim to objectively determine uncertainties of satellite observation- and
124 model simulation-based drought estimations, and in turn to optimally merge any collection of
125 drought indicators in a fully automated statistical framework. With respect to the drought
126 monitoring benchmarks and the reported drought records, the advantages of the optimally
127 objectively blended drought index over the traditional subjectively integrated drought indices are
128 demonstrated. The specifics of the method are described in the next section. The results and
129 validations are then presented in sections 3-5. The potential of applying the method in drought
130 monitoring operation is discussed in section 6, and a brief summary is given in last section.

131 2. Data and Method

132 2.1 Data

133 For this study, we use 6 different SM products. The first is a land surface model estimate
134 of SM from the Noah version 3.2 (referred to as the NLSM). The layer thickness-weighted average
135 of SM estimates in the top three soil layer (0-10 cm; 10-40 cm; 40-100 cm) is used to characterize
136 root zone (0-100 cm) SM. The NLSM simulations were conducted on a near-global gridded
137 domain (from -60°S, -180°W to 90°N, 180°E) at 25 km spatial resolution. The model was spun up
138 by cycling 50 times through the period from 2001 to 2007. Then the simulation was run over the
139 2008-2014 period with one half hour time-step inputs and daily outputs. Atmospheric forcing
140 (Table 2) was taken from 3-hourly 25-km Global Land Data Assimilation System (GLDAS)
141 precipitation (Rodell *et al.*, 2004) and Global Data Assimilation System (GDAS) meteorological
142 data (Derber *et al.*, 1991). Various updates to the specification of vegetation in Noah have been
143 implemented. For example, 2007-2010 Moderate Resolution Imaging Spectroradiometer
144 (MODIS) collection 5 land cover maps and 8-day MODIS leaf area index (LAI)-based green
145 vegetation fraction (GVF) were used to update the climatological fields in Noah (Yin *et al.*, 2015a;
146 Yin *et al.*, 2016).

147 The next drought indicator (Table 2) used in the analysis is the Evaporative Stress Index
148 (ESI), generated with the Atmosphere Land Exchange Inverse (ALEXI) model using land surface
149 temperature data retrieved from satellite thermal infrared imagery (Anderson *et al.*, 1997; 2011).
150 The ESI represents temporal anomalies in the ratio of actual evapotranspiration (ET) to potential
151 ET (PET) and requires no information about antecedent precipitation or subsurface soil
152 characteristics (Anderson *et al.* 2011; Hain *et al.*, 2012). Until recently, ALEXI ESI data
153 production has been limited to areas with high resolution temporal sampling of geostationary
154 sensors (Hain *et al.*, 2016). However, our research team has developed a new and novel method of

155 using twice-daily observations from polar sensors such as MODIS and Visible Infrared Imaging
156 Radiometer Suite (VIIRS) to estimate the mid-morning rise in LST that is used to drive the energy
157 balance estimations within ALEXI. This allows the method to be applied globally using the sensors
158 onboard polar-orbiting satellites rather than a global composite of all available geostationary
159 datasets. The global ALEXI ESI product is available at a spatial resolution of 5 km and a period
160 of record from 2001 to 2014, reprocessed to weekly time-steps and 25-km resolution for this study.

161 Finally, we use four microwave-based SM products (Table 2), referred to as MWSM.
162 These products include SM data from the Advanced Scatterometer (ASCAT, Wagner et al., 1999),
163 WindSat (Li et al., 2010) the Soil Moisture and Ocean Salinity (SMOS, Kerr et al, 2001)
164 instruments, and a blended product from the NOAA Soil Moisture Operational Product System
165 (SMOPS, Yin et al., 2015b). The SMOPS has been developed to process satellite soil moisture
166 observational data at the NOAA National Environmental Satellite, Data, and Information Service
167 (NESDIS) for improving numerical weather prediction models at the NOAA National Weather
168 Service (Yin *et al*, 2014). SMOPS scales the soil moisture data products from the European Space
169 Agency SMOS satellite, ASCAT on EUMETSAT's Metop-A and Metop-B satellites, and WindSat
170 of Naval Research Lab to the climatology of the Noah land surface model, and merges them to a
171 blended global soil moisture data product (Yin *et al*, 2015b). In this study, daily ASCAT, WindSat
172 and SMOPS blended SM products are used from 2008 to 2014, along with SMOS SM data derived
173 during the 2011-2014 period. These global microwave SM retrievals are all at 25 km spatial
174 resolution.

175 Weekly United States Drought Monitor (USDM) data sets from 2008 to 2014 are used to
176 evaluate the performance of the various blended drought indices (BDIs) over the contiguous
177 United States (CONUS). USDM is the drought map that policymakers and media use in

178 discussions of drought and for allocating drought relief, reflecting drought signals conveyed in one
179 or more indices, and reporting impacts and observations from more than 350 contributors around
180 the country (Svoboda *et al.* 2002). In addition, the global BDIs' drought monitoring capabilities
181 are also evaluated against the standard anomalies of the monthly Palmer Drought Severity Index
182 (PDSI) (against the 1985-2014 climatology) at 2.5 degree spatial resolution and the monthly 3-
183 month standardized precipitation evapotranspiration index (SPEI) standard anomalies (against the
184 1985-2014 climatology) at 0.5 degree spatial resolution for the 2008-2014 time period (Vicente-
185 Serrano *et al.*, 2010; Dai *et al.*, 2013). As a landmark in the development of drought indices, PDSI
186 uses readily available temperature and precipitation data to estimate relative dryness and has been
187 reasonably successful at quantifying long-term drought (Dai *et al.*, 2013). SPEI is similar to the
188 standardized precipitation index (SPI), but it includes the role of temperature (Vicente-Serrano *et*
189 *al.*, 2010). SPEI was developed in 2010 and has been used in an increasing number of climatology
190 and hydrology studies (Beguería *et al.*, 2014).

191 2.2 Method

192 The Triple Collocation Error Model (TCEM) assumed that the uncertainties or errors of
193 the three retrieval sources are from mutually distinct sources and are independent from each other
194 (Janssen *et al.*, 2007; Scipal *et al.*, 2008; Miralles *et al.*, 2010; Draper *et al.*, 2013, Pan *et al.*, 2015).
195 In this paper, the TCEM is based on three categories of soil moisture datasets that provide 25 km
196 grid-scale SM estimations: (1) the NLSM, which is subject to errors in the model representation
197 and in the meteorological forcing data; (2) the ALEXI model-based ESI, which does not use any
198 precipitation input, but is sensitive to the accuracy of the thermal infrared (TIR) satellite LST and
199 other model inputs (e.g., vegetation cover, available energy); and (3) the microwave satellite

200 retrievals which is based on land surface microwave radiation physics with error sources being
 201 microwave satellite sensor signal/noise ratio and soil moisture retrieval algorithm accuracy.

202 All of the SM data used in this study were temporally composited over 4-week intervals.
 203 Then the uncertainty or RMSE for each of the four MW SM products was individually computed
 204 in combination with NLSM and ESI in TCEM in order to meet the error independence requirement
 205 of the three data sets used in TCEM. Meanwhile, the NLSM and ESI data sets were evaluated four
 206 times with each corresponding to a different MW SM data set. Their errors were calculated as the
 207 average of the four RMSE values respectively. The climatology of each of the above-mentioned
 208 soil moisture datasets was generated by assembling the variable values for a particular calendar
 209 week for all years of the study periods. Once the climatology was assembled, the standardized
 210 anomalies (ψ) were computed for week w , year y , and grid location (i, j) , as

$$211 \quad \psi(w, y, i, j) = \frac{X(w, y, i, j) - \overline{X(w, i, j)}}{\sigma_x(w, i, j)} \quad (1)$$

212 where \overline{X} and σ_x are climatology and climatological standard deviations for each of the 6
 213 retrievals. Thus, drought estimations for MWSM (ψ_{MWSM}), ESI (ψ_{ESI}) and NLSM (ψ_{NLSM}) are
 214 then expressed as (Janssen *et al.*, 2007; Scipal *et al.*, 2008; Miralles *et al.*, 2010; Draper *et al.*,
 215 2013)

$$216 \quad \begin{aligned} \psi_{\text{MWSM}} &= \Pi + \mu \\ \psi_{\text{ESI}} &= \Pi + \omega \\ \psi_{\text{NLSM}} &= \Pi + \rho \end{aligned} \quad (2)$$

217 where Π indicates the true drought status, and μ , ω and ρ denote the unknown errors in the
 218 MWSM, ESI and NLSM cases. First we assume that the three kinds of errors are uncorrelated
 219 and:

$$220 \quad \mu\rho = 0, \quad \mu\omega = 0, \quad \rho\omega = 0 \quad (3)$$

221 Then the RMSE values for MWSM (ξ_{MWSM}), ESI (ξ_{ESI}) and NLSM (ξ_{NLSM}) are given by
 222 (Stoffelen, 1998; Scipal *et al.*, 2008; Miralles *et al.*, 2010)

$$223 \quad \begin{aligned} \xi_{MWSM} &= (\psi_{MWSM} - \psi_{ESI})(\psi_{MWSM} - \psi_{NLSM}) = \mu^2 \\ \xi_{NLSM} &= (\psi_{NLSM} - \psi_{ESI})(\psi_{NLSM} - \psi_{MWSM}) = \omega^2 \\ \xi_{ESI} &= (\psi_{ESI} - \psi_{NLSM})(\psi_{ESI} - \psi_{MWSM}) = \rho^2 \end{aligned} \quad (4)$$

224 Thus, based on the TCEM, the monthly RMSEs for each of the data sets can be estimated grid by
 225 grid within the global domain.

226 3. Blended Drought Index (BDI)

227 Three techniques for combining the available retrievals into a blended index were
 228 evaluated. These include an equal weighted-average blending, an objectively weighted approach,
 229 and an optimal integration technique. Three blended drought indices are all generated on a near-
 230 global gridded domain (from -60°S, -180°W to 90°N, 180°E) at 25 km spatial resolution over 2008-
 231 2014 time period.

232 3.1 Simple Equal Weighted-Average Blended Drought Index (BDI_s)

233 BDI_s samples all SM products with equal importance. To increase the spatial coverage of
 234 drought estimations, BDI_s integrates all of the six SM retrievals using a weighted-average
 235 blending technique. For the BDI_s, all of the available data sets are assigned the same weight,

236 where the weightings determine the relative importance of each quantity on the average. When the
 237 six SM retrievals are all available, the BDI_s for each pixel within the global domain is

$$238 \quad BDI_{s} = \frac{NLSM + ESI + SMOPS + SMOS + ASCAT + WindSat}{6} \quad (5)$$

239 If an index is missing at a given pixel, the BDI_s is computed as an average of the available
 240 drought estimations.

241 3.2 Objectively Weighted Blended Drought Index (BDI_w)

242 Relative to the BDI_s, the BDI_w treats SM products with lower RMSE as higher quality
 243 data and assigns that dataset a greater weight. Thus, the BDI_w is objectively developed according
 244 to monthly TCEM-based RMSE values computed in Equation (4). And a weight $f(x)$ for an
 245 available index is

$$246 \quad f(x) = \frac{\frac{1}{RMSE_x}}{\sum_{x=1}^N \frac{1}{RMSE_x}} \quad N \in [1,6] \quad (6)$$

247 When the drought assessments are all available, then N is 6, and the BDI_w for each pixel over
 248 the global domain is

$$249 \quad BDI_{w} = f(NLSM) \times NLSM + f(ESI) \times ESI + f(SMOPS) \times SMOPS \\ + f(SMOS) \times SMOS + f(ASCAT) \times ASCAT + f(WindSat) \times WindSat \quad (7)$$

250 Given N values from 1 to 5 in Equation (6), the BDI_w in Equation (7) will be the summation
 251 without counting the unavailable drought estimations.

252 3.3 Optimal Blended Drought Index (BDI_b)

253 The procedure of generating BDI_b for each pixel in the global domain is described in
254 Figure 1. Each pixel is filled by the retrieval that is estimated to have the lowest RMSE based on
255 its TCEM estimate, which ensures that all pixels across the global domain can be covered by the
256 optimal drought estimation information, instead of integrating the evaluations by building their
257 weights. The monthly TCEM-based RMSE for each of the 6 retrievals used here can characterize
258 their time series throughout the year.

259 -----
260 *Please Insert Figure 1 here.*
261 -----

262 4. Evaluation with Benchmark Drought Monitor Products

263 Drought intensity is classified in the USDM into five categories (Table 1) including D0,
264 abnormally dry (percentile < 30%); D1, moderate drought (percentile < 20%); D2, severe drought
265 (percentile < 10%); D3, extreme drought (percentile < 5%); and D4, exceptional drought
266 (percentile < 2%). The statistics of frequency probability for each case here was collected on the
267 global domain over the study period. The large sample size indicates the statistical results here are
268 qualitatively stable and high likely representative of common conditions. Thus, all the indices are
269 classified into 5 categories using the thresholds in Table 1.

270 -----
271 *Please Insert Table 1 here.*
272 -----

273 Based on the assumptions that the drought categories are continuous numbers, Figures 2
274 and 3 show maps describing the temporal correlation between the USDM and each of the drought
275 indices classified using the thresholds in Table 1, which are considered in the inter-comparison of

276 linear correlation in weekly climate-division-based ranking of moisture conditions. The CONUS
277 domain-averaged correlation coefficients (R) for the ASCAT (sample size N = 364, there are 364
278 weeks during the period 2008-2014), SMOS (N = 208, there are 208 weeks during the period 2011-
279 2014), WindSat (N = 364), SMOPS (N = 364), NLSM (N = 364) and ESI (N = 364) retrievals are
280 0.38, 0.11, 0.18, 0.28, 0.40 and 0.35, respectively. The spatial patterns of the correlations between
281 the USDM and the three BDIs agree well (Figure 3). Stronger correlations are observed over the
282 Great Plains and the northeastern United States. These are areas of LST and vegetation indices
283 tending to be anticorrelated, which indicates moisture-limiting vegetation growth conditions
284 (Karnieli et al., 2010). The soil moisture-based BDIs are more sensitive to moisture condition
285 changes. Reduced correlations between USDM and each BDI are observed over parts of the
286 western and eastern US. In southwestern and southeastern US, the moisture changes are driven
287 more by radiation and climate, and thus less tightly coupled with moisture-drought (Anderson et
288 al., 2011). And in northwestern US, the short term precipitation indices used in the USDM may
289 become desynchronized from land surface moisture conditions, because of the hydrologic delays
290 in snowpack-forming regions (Shukla and Wood, 2008). In comparison with the USDM, the
291 average temporal correlation coefficients for BDI_s and BDI_w are 0.36 and 0.34; while the
292 BDI_b yields the highest correlation (R=0.43) in all of the drought estimations.

293 -----
294 *Please Insert Figures 2 and 3 here.*
295 -----

296 Based on 30-year (1985-2014) PDSI means, the correlation coefficients between PDSI
297 standard anomalies and the drought assessments for each of the three BDIs can be found in Figure
298 4. The sample size for each BDI is 84, because there are 84 months during the 2008-2014 period.

299 The higher correlation coefficients for each BDI are found in the areas where the weather stations
300 are relatively dense, such as in the eastern U.S, Australia and portions of Eurasia (Chen et al.,
301 2002; Mu et al., 2013). The correlation coefficients for BDI_s, BDI_w and BDI_b in CONUS
302 (23°~48°N, -125°~-65°E) are 0.45, 0.47 and 0.47, respectively, and in Australia (-40°~-10°N,
303 115°~165°E) are 0.50, 0.53, and 0.59, respectively. The BDI_b (0.48) also yields the highest
304 correlation coefficient in South Africa (-35°~-50°N, -30°~165°E) in comparison with the BDI_s
305 (0.42) and BDI_w (0.44). Relative to BDI_s (0.36) and BDI_w (0.38), the BDI_b (0.40) presents
306 successful to increase the correlation in Eurasia (-10°~55°N, -20°~175°E). In South America (-
307 55°~10°N, -90°~-30°E), the BDI_s (0.35) and BDI_w (0.43) exhibit relatively low correlations
308 with respect to the PDSI standard anomalies, while this situation is significantly improved by the
309 BDI_b (0.48). However, in the areas with weather stations and rain gauges sparsely distributed,
310 the correlations between PDSI and BDIs are relatively low, such as northern Africa and the high
311 latitude areas (Chen et al., 2002; Mu et al., 2013).

312 -----

313 *Please Insert Figures 4 here.*

314 -----

315 With respect to the monthly 0.5 degree 3-month SPEI standard anomalies (against 1985-
316 2014 averages) during the period 2008-2014 (sample size is 84), the correlation coefficients over
317 global domain for each of the three BDIs are exhibited in Figure 5. The higher correlation
318 coefficients for each BDI are shown in CONUS, Europe, Australia, the eastern China and southern
319 South America, where the rain gauges are relatively dense (Chen et al., 2002). The correlation
320 coefficients for BDI_s, BDI_w and BDI_b in CONUS are 0.46, 0.48 and 0.56, respectively, and

321 in Australia are 0.54, 0.58, and 0.59, respectively. Relative to BDI_s (0.33) and BDI_w (0.37), the
322 BDI_b (0.41) presents successful to increase the correlation in Eurasia. The BDI_b (0.40) also
323 yields the highest correlation coefficient in South Africa in comparison with the BDI_s (0.33) and
324 BDI_w (0.37). In South America, the BDI_s (0.27) and BDI_w (0.32) exhibit relatively low
325 correlations with respect to the SPEI standard anomalies, while this situation is improved by the
326 BDI_b (0.37). Similar to Figure 4, the low correlations between SPEI and BDIs can be found in
327 the areas where the weather stations and rain gauges are sparsely, such as Amazon basin, northern
328 Africa and the high latitude areas (Chen et al., 2002; Mu et al., 2013).

329 -----
330 *Please Insert Figures 5 here.*
331 -----

332 5. Evaluation of Drought Events using BDIs

333 BDI performance was also evaluated in relation to reported drought events over the 2009-
334 2014 period (Figure 6). In general, the major annual drought patterns are captured by each BDI
335 product at this coarse time scale. All of the three BDIs can well capture the western Russian
336 drought of 2010 that was very long and intensive, and caused serious damage to the environment
337 and economy (Kogan *et al.*, 2013; Mu *et al.*, 2013) with BDI_s showing a relatively weak signal.
338 And both 2011 Texas drought and the US-Great Plains drought in summer 2012 (Hoerling *et al.*,
339 2014; Otkin *et al.*, 2015) are reasonably represented by the three BDIs, while major differences
340 are noted in 2012 with BDI_s and BDI_w missing drought signals in the Eastern and Southern
341 U.S.

342 According to Australian National Climate Centre (NCC) records (2009a, 2009b), an
343 exceptional drought hit Australia in 2009, which was mitigated by the widespread heavy rainfall

344 throughout northern and central Australia in 2010, while the remaining drought was found in the
345 western Australia (NCC, 2010). Frequent heavy rain events from spring 2010 to autumn 2011, and
346 again in late 2011, lead to Australia's wettest two-year period on record, which was heavily
347 influenced by La Niña conditions (NCC, 2012). During 2013, serious rainfall deficiencies created
348 significant drought conditions that began to develop again and lasted over 2013-2014 period
349 (NCC, 2013, 2014). These documented dry and wet conditions in Australia over 2009-2014 period
350 are effectively exhibited by the annual BDIs (Figure 6) with both BDI_s and BDI_w exhibiting
351 slight drought intensity.

352 Several other extreme droughts, such as 2010 Amazon drought (Lewis *et al.*, 2011; Xu *et*
353 *al.*, 2011; Atkinson *et al.*, 2011) and the continuous droughts during 2009-2012 period in East
354 Africa (Lyon and DeWitt, 2012), are all well captured by the BDI_b [Figure 6(c)]. However,
355 BDI_s tends to reduce drought intensity for above drought episodes and BDI_w cannot reasonably
356 reflect the East Africa drought. In addition, Figure 6(c) illustrates how the western U.S.
357 experienced abnormally dry conditions during the 2013-14 period with the most severe conditions
358 in California, which had been experiencing its worst drought in more than a century
359 (AghaKouchak *et al.*, 2015; Cheng *et al.*, 2015); yet both BDI_s and BDI_w basically miss the
360 drought signals for the California drought event [Figures 6(a) and 6(b)].

361 -----
362 *Please Insert Figure 6 here.*
363 -----

364 The severe drought caused by the great Russian heat wave of 2010 lead to extensive
365 wildfires and thousands of human deaths (Barriopedro *et al.* 2011). The 2010 western Russia
366 drought started in May and lasted through November with response to the record-breaking high

367 temperature caused by a very strong La Niña event (Barriopedro *et al.* 2011; Kogan *et al.*, 2013;
368 Mu *et al.*, 2013). Both BDI_s and BDI_w show the drought event ends in October 2011 with
369 BDI_s showing lower intensity [Figures 7(a) and 7(b)]; while the monthly BDI_b results
370 effectively capture the documented droughts in western Russia in 2010 [Figure 7(c)].

371 -----

372 *Please Insert Figure 7 here.*

373 -----

374 The 2011 drought over the U.S. Southern Great Plains seriously affected agriculture,
375 severely impacted crop and livestock sectors and significantly influenced food prices at the retail
376 level (Grigg, 2014; Arndt and Blunden, 2012; Tadesse *et al.*, 2014) with the state of Texas
377 experiencing its driest year since 1895 (Combs, 2012; Hoerling *et al.*, 2013). This severe drought
378 started in November 2010 and lasted through October 2011, and the dry situation was mitigated
379 across the southeast Texas Panhandle and eastern Rolling plains in November 2011 by heavy
380 precipitation (Combs, 2012; Tadesse *et al.*, 2014). The BDIs are shown to capture the evolution
381 of the 2011 U.S drought with BDI_b providing a more reasonable representation of the observed
382 drought conditions in in October and November 2011 [Figure 8].

383 -----

384 *Please Insert Figures 8 here.*

385 -----

386 The 2013 drought in New Zealand was one of the most extreme on record for this country.
387 During the period of 2012-2013, the dry conditions were unusually widespread across New
388 Zealand, and particularly serious in the North Island (National Institute of Water and Atmospheric
389 Research, 2013a); which reduced agricultural production and cost the national economy at least
390 US\$1.3 billion (Herring *et al.*, 2014). The New Zealand Drought Monitor shows the progression

391 and recession of the drought from October 2012 to May 2013 with the entire New Zealand
392 experiencing the severe drought in March 2013 (National Institute of Water and Atmospheric
393 Research, 2013b). Figures 9(a) and 9(b) show both BDI_s and BDI_w cannot correctly capture the
394 situations of 2012-2013 New Zealand drought events; while the BDI_b in Figure 9(c) perfectly
395 exhibits the drought episodes.

396 -----
397 *Please Insert Figure 9 here.*
398 -----

399 6. Discussion

400 The results shown in Sections 4 and 5 indicate that the BDI_b technique, which objectively
401 integrates drought estimations with the lowest TCEM-based RMSEs, can present more robust
402 capability to track drought development with respect to historical records. However, there are
403 several considerations relevant for interpreting these results. The challenges and opportunities are
404 discussed further here associated with integration approaches and drought characteristics.

405 6.1 Shallow Sensing Depth of Microwave Soil Moisture

406 One issue that must be considered is the shallow sensing depth afforded by the microwave
407 SM products used in this paper. The LSM modeled drought estimates are based on 0-100 cm
408 averages which are much deeper than the top few centimeters sampling depth of the microwave
409 SM-based retrievals. And the ESI represents temporal standardized anomalies in the ratio of actual
410 ET to potential ET (PET), which is also dependent on the root zone SM content related to the
411 rooting depth of the active vegetation (Hain *et al.*, 2009; 2011; Anderson *et al.*, 2015; Otkin *et al.*,
412 2015). In fact, using the surface-only microwave remote sensing product over sparsely vegetated

413 areas is consistent with the properties of NLSM and ESI proxy (Yilmaz *et al.*, 2012); and the
414 potential vertical inconsistencies over densely vegetated areas can be effectively resolved at
415 weekly time scales in terms of the strong linear relation between the surface and the vegetation-
416 adjusted soil moisture simulations in Noah land surface model (Albergel *et al.*, 2008; Yilmaz *et*
417 *al.*, 2012). Although the satellite SM retrievals can only penetrate a few centimeters depth, they
418 represent the fastest response SM dynamics to meteorological anomalies and provide a measure
419 for short-term droughts (Yuan *et al.*, 2015).

420 6.2 Uncertainties from Defining the Errors and the Use of Standardized Anomalies

421 TCEM has been implemented in previous studies using in situ observations, and it shows
422 a surprisingly robust ability of accurate evaluation on the time series (Janssen *et al.*, 2007; Scipal
423 *et al.*, 2008; Miralles *et al.*, 2010; Draper *et al.*, 2013, Pan *et al.*, 2015). The three retrieval sources
424 in this study sufficiently meet the assumption that their errors should be from mutually distinct
425 sources and are not cross-correlated. Prior to the application of TCEM, we transform all the SM
426 time series into standardized anomalies; and their error variances thus are transformed into the
427 same scale, satisfying the assumptions used in the TCEM to quantify the original accuracy for all
428 of the SM retrievals (Miralles *et al.* 2010; Yilmaz *et al.*, 2012; Yilmaz and Crow, 2013). However,
429 with narrowing our focus to drought assessments in this paper, the information content of the SM-
430 based drought estimates can absolutely reflect the possibility that certain products are of higher
431 quality than others (Miralles *et al.* 2010).

432 6.3 Timescale of Compositing Window and Length of Record

433 For this study, composites are generated at 28-day time steps over 4-week moving windows
434 for each of 6 SM retrievals. Across 2011-2014 (SMOS) and 2008-2014 (ASCAT, WindSat and
435 SMOPS) years, the climatologies are based on samples of 112 (28 days \times 4 years) for SMOS and

436 196 (28 days \times 7 years) for ASCAT, WindSat and SMOPS. Additionally, the SM-based BDIs are
437 also validated against PDSI and SPEI standardized anomalies with respect their 1985-2014
438 averages that should well capture climatological distributions. The large sample size and the
439 regarded 30-year PDSI and SPEI averages indicate that the results shown in this paper are
440 qualitatively stable and high likely representative of longer period, although the research periods
441 for SMOS and other three MW SM products are 4-year and 7-year, respectively.

442 6.4 Errors Specific to Individual MW SM Products

443 Microwave remote sensing SM products suffer from the instrument noise and uncertainty
444 in microwave emission modeling, which hampers their use in operational drought monitoring. The
445 ASCAT SM-based drought estimations exhibit higher correlations with the USDM data sets at the
446 regional scale and the PDSI and SPEI products on a global domain in comparison with the passive
447 microwave SM products including WindSat and SMOS. This suggests that the weights of the
448 active SM signals should be increased to enhance the drought monitoring capabilities of the
449 blended products that integrate satellite SM retrievals from multiple single sensors. However,
450 active microwave sensors such as ASCAT, have been shown to have greater uncertainty over high-
451 elevation areas (Wagner *et al.*, 2013), which leads to the modest ASCAT performance (e.g., central
452 Asia). The error propagation for the remotely sensed SM products can be easily tracked in the
453 weighting-based BDI_s and BDI_w datasets with BDI_s being significantly impacted, while this
454 kind of uncertainty is unreasonably identified in BDI_b maps. Using uniform weighting, the BDI_s
455 is determined by the relative importance of each quantity on the average. The improvements
456 related to the use of high quality data and degradations related to datasets with poor retrieval
457 quality have equal opportunities to impact the BDI_s capabilities in monitoring drought events.
458 Although BDI_w is objectively developed according to TCEM RMSE-based weights and the

459 fractions of high (low) quality signals are increased (decreased), the lower weights of drought
460 evaluations that have larger uncertainties can still strongly degrade BDI_w's performance.
461 Relative to weights-based BDI_s and BDI_w, the BDI_b can merge the drought estimation that
462 has lower uncertainty with ignoring the poor representation of the soil moisture condition.

463 6.5 Seasonal Issues

464 Drought monitoring and warning studies are generally focused on the drought events
465 occurred during the growing season; however, recent studies have claimed that much more
466 attention should be paid to cold season droughts since their occurrence and intensity are increasing,
467 such as the California drought during November-April winters of 2011/12–2013/14, the 2010-
468 2012 China Southwest drought, and consecutive and worsening winter drought conditions in Nepal
469 during 2000-2009 period (Wang *et al.*, 2013; Yin *et al.*, 2015a; Seager *et al.*, 2015). However, the
470 remotely sensed observations used in drought monitoring are greatly hampered by the frozen soil
471 and low evapotranspiration, which can lead to the poor performance of weights-based BDI_s and
472 BDI_w in cold season with missing the drought signals. This situation can be significantly
473 improved by BDI_b with integrating the drought assessments that can exhibit the lowest TCEM-
474 based RMSE values. The statistical results show that the satellite SM signals assembled into BDI_b
475 are around 12%, 22%, 29% and 25% in winter (December, January and February), spring (March,
476 April and May), summer (June, July and August) and autumn (September, October and
477 November), respectively with shifting their detection toward North in the warm season (April-
478 September) and toward South during October-March period.

479 6.6 Additional future works

480 a. Development of Finer Resolution BDI_b

481 Microwave satellite sensors have proven to be effective for remotely-sensed SM because of
 482 the large contrast of dielectric properties between liquid water and dry soil (Wang et al., 1980;
 483 Njoku and Kong, 1997). However, because of the current limitation of satellite antenna
 484 technology, the spatial resolutions of the microwave SM products are generally tens of kilometers.
 485 To overcome the coarse spatial scale limitation of relatively accurate microwave SM data, several
 486 downscaling algorithms have been proposed in recent literatures (Merlin et al., 2006; Narayan et
 487 al, 2006; Zhan et al, 2006; Piles et al, 2011; Parinussa et al, 2014, Peng et al, 2016). Additionally,
 488 the land surface temperature can be retrieved from thermal infrared imagery over a broad range of
 489 spatiotemporal resolutions from several meters to couple kilometers, which allows developing the
 490 finer spatial resolution ESI product on the whole global domain (Anderson et al., 2014; Hain et
 491 al., 2017). Based on the downscaled satellite SM products and the tens of meters ESI data, the finer
 492 spatial resolution BDI_b in drought occurrence areas, which can provide much more details for
 493 decision makers, is expected to be developed in near future.

494 b. Integrating More Available Drought Evaluations

495 We proposed to objectively integrate the SM satellite observations and model simulations
 496 based on quantitative evaluations of their uncertainties derived from the TCEM. TCEM requires
 497 three data sets with their errors totally independent from each other. This requirement will be met
 498 by selecting two independent data sets as anchors and use them to evaluate other data sets that are
 499 independent from the two anchor data sets and probably similar to each other. Thus we will have
 500 the general form for Equations (2-4):

$$\begin{aligned}
 \psi_{\alpha 1} &= \Pi + \mu^* \\
 \psi_{\alpha 2} &= \Pi + \omega^* \\
 \psi_e &= \Pi + \rho^*
 \end{aligned}
 \tag{5}$$

502 where $\psi_{\alpha 1}$, $\psi_{\alpha 2}$ and ψ_e are the standardized anomalies of the two anchor data sets and the
 503 evaluating product, respectively; and μ^* , ω^* and ρ^* are the corresponding unknown errors. With
 504 assumption the three kinds of errors are uncorrelated ($\mu^*\rho^*=0$, $\mu^*\omega^*=0$, $\rho^*\omega^*=0$), their
 505 RMSE values can be given by

$$\begin{aligned}
 \xi_{\alpha 1} &= (\psi_{\alpha 1} - \psi_{\alpha 2})(\psi_{\alpha 1} - \psi_e) = \mu^{*2} \\
 \xi_{\alpha 2} &= (\psi_{\alpha 2} - \psi_{\alpha 1})(\psi_{\alpha 2} - \psi_e) = \omega^{*2} \\
 \xi_e &= (\psi_e - \psi_{\alpha 1})(\psi_e - \psi_{\alpha 2}) = \rho^{*2}
 \end{aligned}
 \tag{6}$$

507 Specifically, for agricultural drought—the water deficit is the negative soil moisture anomaly
 508 that crop could not tolerate (Wilhite and Glantz, 1985; Anderson et al., 2011), the LSM simulations
 509 and the thermal infrared/near-infrared satellite observations-based ESI/Vegetation Health Index
 510 (Kogan, 1997) can be used as the anchors. Current existing and upcoming microwave SM products
 511 and in situ SM measurements are thus able to be quantitative evaluated, and in turn to be
 512 objectively integrated toward the BDI_b.

513 In recent years, increased attention has also been paid to the role of previously neglected water
 514 source (e.g., irrigation, water storage) processes on the surface energy balance, since traditional
 515 soil water balance modeling is only based on vertical water flow and neglecting secondary water
 516 source due to processes (Hain et al., 2015; Kumar et al., 2016). Thus time series datasets of existing
 517 meteorological (e.g., satellite precipitation) and hydrological (e.g., satellite irrigation/water
 518 storage retrievals) drought monitoring indicators will be scaled to their standard anomalies.
 519 Based on quantitative evaluations of the TCEM-based uncertainties, short- and long-term BDI_b
 520 products are expected to be further improved with integrating meteorological and hydrological
 521 drought assessments, respectively.

522 7. Conclusions

523 We integrated the commonly used satellite SM products, ALEXI-based ESI and LSM
524 simulations into a subjective BDI_s and two objective BDIs (BDI_w and BDI_b) based on
525 quantitative evaluations of the relative uncertainties of these products derived from a TCEM.
526 Performance of the three BDIs was analyzed in comparison with drought monitoring benchmarks
527 and the official drought records. BDI_s using the subjective weighting exhibits modest
528 performance with trending to underestimate drought intensity. Relative to the weighting-based
529 BDI_s and BDI_w, the BDI_b can more reasonably measure drought severity according to
530 intensity and duration, and can provide better capability to identify the onset and end of drought
531 episodes. Over the BDI_s and BDI_w, the BDI_b presents an advantage of higher consistence with
532 the climatological PDSI and SPEI datasets and current operational USDM product. In addition to
533 operational insights, the BDI_b is recommended as an indicator which can merge new upcoming
534 satellite SM products and more available drought evaluations when they can respect to the TCEM
535 assumptions.

536 Acknowledgements

537 This work was supported by a grant from NOAA JPSS Proving Ground and Risk Reduction
538 (PGRR) Program and by a grant from the NASA Applied Sciences Water Resource Program
539 (Award number: NNX12AK90G). SMOPS soil moisture data product could be obtained from
540 NOAA-NESDIS at http://www.ospo.noaa.gov/Products/land/smops/smops_loops.html. We
541 would like to thank Dr. Aiguo Dai for providing the PDSI data. The 3-month SPEI data can be
542 obtained from: <https://climatedataguide.ucar.edu/climate-data/standardized-precipitation->

543 evapotranspiration-index-spei. We are also grateful to the anonymous reviewers for helping
544 significantly improve the quality of the manuscript.

545

546

547

548

549 Reference

550 AghaKouchak A., Feldman D., Hoerling M., Huxman T., Lund J., 2015, Recognize Anthropogenic
551 Drought, *Nature*, 524 (7566), 409-4011, doi:10.1038/524409a

552 Albergel, C., Rüdiger, C., Pellarin, T., Calvet, J.-C., Fritz, N., Froissard, F., Suquia, D., Petitpa,
553 A., Piguet, B., and Martin, E.: From near-surface to root-zone soil moisture using an
554 exponential filter: an assessment of the method based on in-situ observations and model
555 simulations, *Hydrol. Earth Syst. Sci.*, 12, 1323-1337, doi:10.5194/hess-12-1323-2008,
556 2008.

557 Anderson M C., C Hain, J Otkin, X Zhan, K Mo, M Svoboda, B Wardlow, and A Pimstein, 2013:
558 An Intercomparison of Drought Indicators Based on Thermal Remote Sensing and
559 NLDAS-2 Simulations with U.S. Drought Monitor Classifications. *J. Hydrometeor*, 14,
560 1035–1056.

561 Anderson M. C., C. R. Hain, B. D. Wardlow, A. Pimstein, J. R. Mecikalski and W. P. Kustas,
562 2011: Evaluation of drought indices based on thermal remote sensing of evapotranspiration
563 over the continental United States. *J. of Climate*, 24, 2025-2044.

564 Anderson M.C., Zolin C A., C R. Hain, K Semmens , M. T Yilmaz, F Gao, 2015, Comparison of
565 satellite-derived LAI and precipitation anomalies over Brazil with a thermal infrared-based
566 Evaporative Stress Index for 2003-2013. *J. Hydrol.*, 526, 287-302

567 Anderson MC, C Hain, F Gao, KA Semmens, Y Yang, MA Schull, T Ring, WP Kustas, JG Alfieri.
568 2014. Scaling Surface Fluxes from Tower Footprint to Global Model Pixel Scale Using
569 Multi-Satellite Data Fusion, AGU Fall Meeting Abstracts: 2014AGUFM.B52A. 02A

570 Anderson, M. C., Norman, J. M., Diak, G. R., Kustas, W. P., and Mecikalski, J. R.: A two-source
571 time-integrated model for estimating surface fluxes using thermal infrared remote sensing,
572 *Remote Sens. Environ.*, 60, 195–216, 1997.

573 Anne Steinemann, Sam F. Iacobellis, and Daniel R. Cayan, 2015: Developing and Evaluating
574 Drought Indicators for Decision-Making. *J. Hydrometeor*, 16, 1793–1803.

575 Arndt D.S., and J. Blunden, 2012: State of the climate in 2011. *Bulletin of the American*
576 *Meteorological Society*, 93: S1-S280.

577 Atkinson P. M., J. Dash, and C. Jeganathan, 2011: Amazon vegetation greenness as measured by
578 satellite sensors over the last decade. *Geophys. Res. Lett.*, 38, L19105,
579 doi:10.1029/2011GL049118.

580 Azmi M., C. R€udiger, and J. P. Walker (2016), A data fusion-based drought index, *Water Resour.*
581 *Res.*, 52, 2222–2239, doi:10.1002/2015WR017834.

582 Barriopedro, D., E. M. Fischer, J. Luterbacher, R. M. Trigo, and R. García-Herrera, 2011: The hot
583 summer of 2010: Redrawing the temperature record map of Europe. *Science*, 332, 220–
584 224.

585 Beguería S, S M. Vicente-Serrano, F Reig, B Latorre. Standardized precipitation
586 evapotranspiration index (SPEI) revisited: parameter fitting, evapotranspiration models,
587 tools, datasets and drought monitoring. *Int. J. Climatol.* 34: 3001–3023 (2014).

588 Bolten, J. D., and W. T. Crow (2012), Improved prediction of quasi-global vegetation conditions
589 using remotely-sensed surface soil moisture, *Geophys. Res. Lett.*, 39, L19406,
590 doi:10.1029/2012GL053470.

591 Chen, M., P. Xie, J. E. Janowiak, and P. A. Arkin, 2002: Global land precipitation: A 50-yr
592 monthly analysis based on gauge observations. *J. Hydrometeor.*, 3, 249–266

593 Cheng L., Hoerling M., AghaKouchak A., Livneh B., Quan X.-W., Eischeid J., 2015, How Has
594 Human-induced Climate Change Affected California Drought Risk?, *J. Climate*, 29(1):
595 111–120., doi: 10.1175/JCLI-D-15-0260.1.

596 Combs, S., 2012: The Impact of the 2011 Drought and Beyond. Texas Comptroller of Public
597 Accounts Special Report, Publication 96-1704 [available online at
598 <http://www.window.state.tx.us/specialrpt/drought/>].

599 Crow W. T., S. V. Kumar, and J. D. Bolten. 2012. On the utility of land surface models for
600 agricultural drought monitoring, *Hydrology and Earth System Sciences Discussions*, 9:
601 5167-5193.

602 Crow, W. T., and E. Wood, 2003: The assimilation of remotely sensed soil brightness temperature
603 imagery into a land surface model using ensemble Kalman filtering: A case study based on
604 ESTAR measurements during SGP97. *Adv. Water Resour.*, 26, 137–149.

605 Dai A, Increasing drought under global warming in observations and models, *Nature Climate*
606 *Change*, 2013(3): 52-58

607 Dai Y., Zeng X., Dickinson R.E., Baker I., Bonan G.B., Bosilovich M.G., Denning A.S., Dirmeyer
608 P.A., Houser P.R., Niu G., Oleson K.W., Schlosser C.A., Yang Z., (2003), The Common
609 Land Model. *Bulletin of the American Meteorological Society*, DOI: 10.1175/BAMS-84-
610 8-1013.

611 Draper C., R. Reichle, R. De Jeu, V. Naeimi, R. Parinussa, W. Wagner. 2013, Estimating root
612 mean square errors in remotely sensed soil moisture over continental scale domains.
613 *Remote Sensing of Environment*, 137: 288-298

614 Ek, M. B., K. E. Mitchell, Y. Lin, E. Rogers, P. Grunmann, V. Koren, G. Gayno, and J. D. Tarpley,
615 2003: implementation of Noah land surface model advances in the National Centers for
616 Environmental Prediction operational mesoscale Eta model, *J. Geophys. Res.*, 108(D22),
617 8851, doi:10.1029/2002JD003296.

618 Grigg, N.S., 2014: The 2011–2012 drought in the United States: New lessons from a record event.
619 *International Journal of Water Resources Development*, 30(2): 183-199.

620 Hain C. R., W. T. Crow, M. C. Anderson, J. R. Mecikalski. 2012. An ensemble Kalman filter dual
621 assimilation of thermal infrared and microwave satellite observations of soil moisture into
622 the Noah land surface model. *Water Resources Research*, 48, W11517,
623 doi:10.1029/2011WR011268.

624 Hao Z., A Aghakouchak, N Nakhjiri, A Farahmand. Global integrated drought monitoring and
625 prediction system. *Sci. Data* 1:140001 doi: 10.1038/sdata.2014.1 (2014).

626 Hao, Z., AghaKouchak, A., 2013, Multivariate standardized drought index: a parametric multi-
627 index model. *Adv. Water Resour.* 57: 12–18.

628 Hao, Z., Hong, Y., Xia, Y., Singh, V. P., Hao, F., & Cheng, H. (2016). Probabilistic drought
629 characterization in the categorical form using ordinal regression. *Journal of Hydrology*,
630 535, 331-339.

631 Hao, Z., V. P. Singh, 2015, Drought characterization from a multivariate perspective: A review.
632 *Journal of Hydrology*, 527: 668–678

633 Heim, R. R., Jr., 2002, A review of twentieth-century drought indices used in the United States,
634 *Bull. Am. Meteorol. Soc.*, 83, 1149–1165.

635 Herring, S.C., Hoerling, M.P., Peterson, T.C., Stott, P.A. (Eds.), 2014. Explaining extreme events
636 of 2013 from a climate perspective. *Bull. Am. Meteorol. Soc.* 95 (9), S1–S96

637 Hoerling M., J. Eischeid, A. Kumar, R. Leung, A. Mariotti, K. Mo, S. Schubert, and R. Seager,
638 2014: Causes and Predictability of the 2012 Great Plains Drought. *Bull. Amer. Meteor.*
639 *Soc.*, 95, 269–282.

640 Janssen, P., S. Abdalla, H. Hersbach, and J.-R. Bidlot (2007), Error estimation of buoy, satellite,
641 and model wave height data, *J. Atmos. Oceanic Technol.*, 24, 1665-1677.

642 Kao, S.C., R. S. Govindaraju, 2010, A copula-based joint deficit index for droughts. *J. Hydrol.*,
643 380 (1–2): 121–134.

644 Karnieli, A., N. Agam, R. T. Pinker, M. C. Anderson, M. L. Imhoff, G. G. Gutman, N. Panov, and
645 A. Goldberg, 2010: Use of NDVI and land surface temperature for drought assessment:
646 Merits and limitations. *J. Climate*, 23, 618–633.

647 Kerr Y H., P. Waldteufel, J-P Wigneron, J-M Martinuzzi, J Font, and M Berger. Soil Moisture
648 Retrieval from Space: The Soil Moisture and Ocean Salinity (SMOS) Mission. IEEE
649 Transactions on Geoscience and Remote Sensing, 2001, 39(8): 1729-1735.

650 Keyantash, J.A., Dracup, J.A., 2004, An aggregate drought index: assessing drought severity
651 based on fluctuations in the hydrologic cycle and surface water storage. Water Resour.
652 Res., 40 (9): W09304.

653 Kogan F, T Adamenko & W Guo (2013) Global and regional drought dynamics in the climate
654 warming era, Remote Sensing Letters, 4:4, 364-372.

655 Kogan F., 1997, Global drought watch from space. Bull. Am. Meteorol. Soc., 78:621–636.

656 Hain, C. R., W. T. Crow, M. C. Anderson, M. T. Yilmaz, 2015, Diagnosing Neglected Soil
657 Moisture Source–Sink Processes via a Thermal Infrared–Based Two-Source Energy
658 Balance Model. J. Hydrometeorol.,16: 1070-1086.

659 Koster R D, Suarez M J, Ducharne A, et al. 2000. A catchmentbased approach to modeling land
660 surface processes in a general circulation model 1. Model structure. J Geophys Res,
661 105(D20):809 - 822.

662 Koster R. D., Z. Guo, R. Yang, P. A. Dirmeyer, K. Mitchell, and M. J. Puma, 2009: On the nature
663 of soil moisture in land surface models. J. Climate, 22, 4322–4325

664 Kowalczyk E A, Wang Y P, Law R M, et al. 2006. CSIRO Atmosphere Biosphere Land
665 Exchange model for use in climate models and as an offline model. CSIRO Technical
666 Report, 37.

667 Kumar, S. V., B. F. Zaitchik, C. D. Peters-Lidard, et al. (2016), Assimilation of gridded GRACE
668 terrestrial water storage estimates in the North American Land Data Assimilation System.
669 J. Hydrometeorol., 17, 1951–1972, doi:10.1175/JHM-D-15-0157.

670 Kumar, S. V., R. H. Reichle, R. D. Koster, W. T. Crow, and C. D. Peters-Lidard, 2009: Role of
671 subsurface physics in the assimilation of surface soil moisture observations. J.
672 Hydrometeor., 10, 1534–1547

673 Lewis S.L., Brando P.M., Phillips O.L., Van der Heijden G.M.F., Nepstad D., 2011, The 2010
674 Amazon Drought. Science, 2011, 331: 554

675 Li, L, Gaiser P W., B-C Gao, Bevilacqua R M, Jackson T J, Njoku E G, Rudiger C, Calvet J-C,
676 Bindlish R. WindSat Global Soil Moisture Retrieval and Validation. IEEE Transactions on
677 Geoscience and Remote Sensing, 2010, 48(5): 2224-2241.

678 Liu, Y. Y., R. M. Parinussa, W. A. Dorigo, R. A. M. De Jeu, W. Wagner, A. I. J. M. van Dijk, M.
679 F. McCabe, and J. P. Evans, 2011: Developing an improved soil moisture dataset by
680 blending passive and active microwave satellite-based retrievals. Hydrol. Earth Syst. Sci.,
681 15, 425–436, doi:10.5194/hess-15-425-2011.

682 Lyon, B., and D. G. DeWitt, 2012: A recent and abrupt decline in the East African long rains.
683 *Geophys. Res.Lett.*, 39, L02702, doi:10.1029/2011GL050337.

684 Mazdhyasni O, A AghaKouchak, 2015, Substantial increase in concurrent droughts and heatwaves
685 in the United States. Proceedings of the National Academy of Sciences, 112(37): 11484-
686 11489

687 McNally A., G. Husak, M. Brown, M. Carroll, C. Funk, S. Yatheendradas, K. Aresenault, C.
688 Peters-Lidard, and J. Verdin, 2015: Calculating Crop Water Requirement Satisfaction in
689 the West Africa Sahel with Remotely Sensed Soil Moisture. *J. Hydrometeor.*
690 doi:10.1175/JHM-D-14-0049.1

691 Merlin, O., G. Chehbouni, Y. Kerr, D. Goodrich, 2006, A downscaling method for distributing
692 surface soil moisture within a microwave pixel: Application to the Monsoon'90 data.
693 *Remote Sensing of Environment*, 101, 379–389.

694 Miralles D G., W T. Crow, and M H. Cosh, 2010: Estimating Spatial Sampling Errors in Coarse-
695 Scale Soil Moisture Estimates Derived from Point-Scale Observations. *J.*
696 *Hydrometeor*, 11, 1423-1429

697 Mu Q, M Zhao, J S. Kimball, N G. McDowell, and S W. Running, 2013: A Remotely Sensed
698 Global Terrestrial Drought Severity Index. *Bull. Amer. Meteor. Soc.*, 94, 83–98.

699 Naeimi V., Scipal K., Bartalis Z., Hasenauer S., Wagner W. (2009). An improved soil moisture
700 retrieval algorithm for ERS and METOP scatterometer observations. *IEEE Transactions*
701 *on Geoscience and Remote Sensing*, 47(7), 1999-2013.

702 Narayan, U., V. Lakshmi, T.H. Jackson, 2006, High-resolution change estimation of soil moisture
703 using L-band radiometer and radar observations made during the SMEX02 experiments.
704 *IEEE Transactions on Geoscience and Remote Sensing*, Vol. 44: 1545-1554/

705 National Climate Centre, 2009a: Exceptional winter heat over large parts of Australia. Bureau of
706 Meteorology Special Climate Statement 18: 2-13.

707 National Climate Centre, 2009b: A prolonged spring heatwave over central and south-eastern
708 Australia. Bureau of Meteorology Special Climate Statement 19: 2-17.

709 National Climate Centre, 2010: An exceptionally wet Dry Season 2010 in northern and central
710 Australia. Bureau of Meteorology Special Climate Statement 23: 2-6.

711 National Climate Centre, 2012: Australia's wettest two-year period on record; 2010–2011. Bureau
712 of Meteorology Special Climate Statement 38: 2-9.

713 National Climate Centre, 2013: Australia's warmest September on record. Bureau of Meteorology
714 Special Climate Statement 46: 1-9.

715 National Climate Centre, 2014: Australia's warmest spring on record. Bureau of Meteorology
716 Special Climate Statement 50: 1-7.

717 National Institute of Water and Atmospheric Research, 2013a, 2012-13 drought: a summary: 1-2

718 National Institute of Water and Atmospheric Research, 2013b, The 2012-13 drought: an
719 assessment and historical perspective: 6-34

720 Nearing G. S., D. M. Mocko, C. D. Peters-Lidard, et al., 2016, "Benchmarking NLDAS-2 soil
721 moisture and evapotranspiration to separate uncertainty contributions," *J. Hydrometeorol.*,
722 17: 745-759

723 Njoku E. G., J-A Kong, 1997, Theory for Passive Microwave Remote Sensing of Near Surface
724 Soil Moisture. *J. Geophys. Res.*, 82(20): 3109-3118

725 Njoku, E. G., T. J. Jackson, V. Lakshmi, T. K. Chan, and S. V. Nghiem, 2003: Soil moisture
726 retrieval from AMSR-E. *IEEE Trans. Geosci. Remote Sens.*, 41, 215–229

727 Oleson K W, Dai Y, Bonan G, et al. 2004. Technical description of the community land model
728 (CLM). NCAR Technical Note NCAR/TN- 461 + STR, National Center for Atmospheric
729 Research Boulder, Colorado.

730 Otkin J A., Mark Shafer, Mark Svoboda, Brian Wardlow, Martha C. Anderson, Christopher Hain,
731 and Jeffrey Basara, 2015: Facilitating the Use of Drought Early Warning Information
732 through Interactions with Agricultural Stakeholders. *Bull. Amer. Meteor. Soc.*, 96, 1073–
733 1078.

734 Parinussa, R. M., M. T. Yilmaz, M. C. Anderson, C. R. Hain, and R. A. M. de Jeu, 2014, An
735 intercomparison of remotely sensed soil moisture products at various spatial scales over
736 the Iberian Peninsula. *Hydrol. Processes*, 28 (18), 4865-4876

737 Peng J., A. Loew, S. Zhang, J. Wang, and J. Niesel, 2016, Spatial Downscaling of Satellite Soil
738 Moisture Data Using a Vegetation Temperature Condition Index. *IEEE T. Geosci. Remote*,
739 54: 558–566.

740 Piles, M., A. Camps, M. Vall-Llossera, I. Corbella, R. Panciera, C. Rüdiger, Y. H. Kerr, J. Walker,
741 2011, Downscaling SMOS Derived Soil Moisture Using MODIS Visible/Infrared Data.
742 *IEEE T. Geosci. Remote*, 49: 3156–3166.

743 Pozzi W., and Coauthors, 2013: Toward global drought early warning capability: Expanding
744 international cooperation for the development of a framework for monitoring and
745 forecasting. *Bull. Amer. Meteor. Soc.*, 94, 776–785.

746 Rajsekhar, D., Singh, V.P., Mishra, A.K., 2015, Multivariate drought index: an information
747 theory based approach for integrated drought assessment. *J. Hydrol.* 526: 164–182.

748 Reichle R. H., and R. D. Koster, 2004: Bias reduction in short records of satellite soil moisture.
749 Geophys. Res. Lett., 31, L19501, doi:10.1029/2004GL020938.

750 Grumm R H. and R Hart, 2001: Standardized Anomalies Applied to Significant Cold Season
751 Weather Events: Preliminary Findings. *Wea. Forecasting*, 16, 736–754.

752 Scipal, K., T. Holmes, R. de Jeu, V. Naeimi, and W. Wagner (2008), A possible solution for the
753 problem of estimating the error structure of global soil moisture data sets, *Geophys. Res.*
754 *Lett.*, 35, L24403, doi:10.1029/2008GL035599.

755 Seager, R., M. Hoerling, S. Schubert, H. Wang, B. Lyon, A. Kumar, J. Nakamura, and N.
756 Henderson, 2015: Causes of the 2011-14 California drought. *J. Climate*, 28, 6997–7024.

757 Sheffield J, E F. Wood, N Chaney, K Guan, S Sadri, X Yuan, L Olang, A Amani, A Ali, S Demuth,
758 and L Ogallo, 2014: A Drought Monitoring and Forecasting System for Sub-Sahara
759 African Water Resources and Food Security. *Bull. Amer. Meteor. Soc.*, 95, 861–882.

760 Shukla, S., and A. W. Wood, 2008: Use of a standardized runoff index for characterizing
761 hydrologic drought. *Geophys. Res. Lett.*, 35, L02405, doi:10.1029/2007GL032487.

762 Stoffelen, A. (1998). Toward the true near-surface wind speed: Error modeling and calibration
763 using triple collocation. *Journal of Geophysical Research*, 7755-7766.

764 Svoboda, M., D Lecomte, M. Hayes., et al., 2002, The drought monitor, *Bull. Am. Meteorol. Soc.*,
765 83, 1181–1190.

766 Tadesse T, B D. Wardlow, J F. Brown, M D. Svoboda, M J. Hayes, B Fuchs, and D Gutzmer,
767 2015: Assessing the Vegetation Condition Impacts of the 2011 Drought across the U.S.

768 Southern Great Plains Using the Vegetation Drought Response Index (VegDRI). *J. Appl.*
769 *Meteor. Climatol.*, 54, 153–169. doi: <http://dx.doi.org/10.1175/JAMC-D-14-0048.1>

770 Tarhule, A., and P. J. Lamb, 2003: Climate research and seasonal forecasting for West Africans:
771 Perceptions, dissemination, and use? *Bull. Amer. Meteor. Soc.*, 84, 1741–1759.

772 Vicente-Serrano S M., S Beguería, and J I. López-Moreno. 2010, A Multiscalar Drought Index
773 Sensitive to Global Warming: The Standardized Precipitation Evapotranspiration Index.
774 *Journal of Climate*, 23: 1696-1718

775 Wagner W., Hahn S., Kidd R., Melzer T., Bartalis Z., Hasenauer S., et al. (2013). The ASCAT soil
776 moisture product: A review of its specifications, validation results, and merging
777 applications. *Meteorologische Zeitschrift*, 22, 5-33

778 Wagner, W., Lemoine G., Rott H., 1999, A method for estimating soil moisture from ERS
779 scatterometer and soil data. *Remote Sensing of Environment*, 70: 191-207.

780 Wang J. R., T. J. Schmugge, 1980, An Empirical Model for the Complex Dielectric Permittivity
781 of Soils AS a Function of Water Content. *IEEE Transactions on Geoscience and Remote*
782 *Sensing*, GE-18(4): 288-295.

783 Wang S-Y, J-H Yoon, R R. Gillies, C Cho. 2013, What Caused the Winter Drought in Western
784 Nepal during Recent Years. *Journal Climate*, 26: 8241-8256.

785 Wang, H., J. Rogers, and D. Munroe, 2015: Commonly Used Drought Indices as Indicators of Soil
786 Moisture in China. *J. Hydrometeor.* doi:10.1175/JHM-D-14-0076.

787 Wilhite, D. A., and M. H. Glantz, 1985: Understanding the drought phenomenon: The role of
788 definitions. *Water Int.*, 10: 111–120.

789 Xia Y., K. Mitchell, M. EK, J. Sheffield, B. Cosgrove, E. Wood, L. Luo, C. Alonge, H. Wei, J.
790 Meng, B. Livneh, D. Lettenmaier, V. Koren, Q. Duan, K. Mo, Y. Fan, D. Mocko. 2012.
791 Continental-scale water and energy flux analysis and validation for the North American
792 Land Data Assimilation System project phase 2 (NLDAS-2): 1. Intercomparison and
793 application of model products. *Journal of Geophysical Research*, 117, D03109, doi:
794 10.1029/2011JD016048.

795 Xia, Y., M. B. Ek, C. D. Peters-Lidard, D. Mocko, M. Svoboda, J. Sheffield, and E. F. Wood
796 (2014), Application of USDM statistics in NLDAS-2: Optimal blended NLDAS drought
797 index over the continental United States, *J. Geophys. Res. Atmos.*, 119, 2947–2965,
798 doi:10.1002/2013JD020994.

799 Xu L., A. Samanta, M. H. Costa, S. Ganguly, R. R. Nemani, and R. B. Myneni, 2011: Widespread
800 decline in greenness of Amazonian vegetation due to the 2010 drought. *Geophys. Res.*
801 *Let.*, 38, L07402, doi:10.1029/2011GL046824.

802 Yang R, Cohn S E, da Silva A, et al. 2003. Tangent linear analysis of the Mosaic land surface
803 model. *J Geophys Res: Atmospheres*, 108(D2): 4054. DOI:10. 1029/2002JD002410.

804 Yilmaz, M.T. and W.T. Crow, "The optimality of potential rescaling approaches in land data
805 assimilation" *Journal of Hydrometeorology*, 14, 650-660, 10.1175/JHMD12052.1, 2013.

806 Yilmaz, M.T., W.T. Crow, M.C. Anderson and C. Hain, "An objective methodology for merging
807 satellite and model-based soil moisture products," *Water Resources Research*, 48, W11502,
808 10.1029/2011WR011682, 2012.

809 Yin J., X. Zhan, Y. Zheng, C. Hain, J. Liu, L. Fang, 2015c, Optimal ensemble size of Ensemble
810 Kalman Filter in sequential soil moisture data assimilation of land surface model. *Geophys.*
811 *Res. Lett.*, 16(28): 6710-6715

812 Yin J., X. Zhan, Y. Zheng, J. Liu, C. R. Hain, and L. Fang (2014), Impact of quality control of
813 satellite soil moisture data on their assimilation into land surface model, *Geophys. Res.*
814 *Lett.*, 41, 7159-7166, doi:10.1002/2014GL060659.

815 Yin J., X. Zhan, Y. Zheng, J. Liu, L. Fang, and C. R. Hain. 2015b. Enhancing Model Skill by
816 Assimilating SMOPS Blended Soil Moisture Product into Noah Land Surface Model.
817 *Journal of Hydrometeorology*, 16(2): 917-931

818 Yin J., Y. Zheng, X. Zhan, C. Hain, Q Zhai, C Duan, R Wu, J. Liu, L. Fang. An assessment of
819 impacts of surface type changes on drought monitoring.
820 *International Journal of Remote Sensing*. 2015a, 36(24): 6116-6134.

821 Yin, J., X. Zhan, Y Zheng, C. Hain, M. EK, J Wen, L Fang, J Liu. 2016. Improving Noah Land
822 Surface Model Performance using Near Real Time Surface Albedo and Green Vegetation
823 Fraction, *Agricultural and Forest Meteorology*, 218-219: 171-183

824 Yuan, X., Z. Ma, M. Pan, and C. Shi (2015), Microwave remote sensing of short-term droughts
825 during crop growing seasons, *Geophys. Res. Lett.*, 42, doi:10.1002/2015GL064125.

826 Zhan X., W. Zheng, J. Meng, J. Dong, and M. EK. 2012. Impact of SMOS soil moisture data
827 assimilation on NCEP-GFS forecasts. *Geophysical Research Abstracts*, 14: EGU2012-
828 12724-1.

829 Zhan, X., P. R. Houser, J.P. Walker, W. Crow, 2006, A method for retrieving high resolution
 830 soilmoisture from Hydros L-Band radiometer and radar observations. IEEE Transactions
 831 on Geoscience and Remote Sensing, Vol. 44. No. 6: 1534-1544.

832 Zhang X., N Chen, J Li, Z Chen, D Niyogi, 2017, Multi-sensor integrated framework and index
 833 for agricultural drought monitoring. Remote Sensing of Environment, 188: 141–163

834

835

836

837

838

839

840 Table 1. Drought severity information in the original standardized scale.

Categories	NLSM	ESI	ASCAT	SMOS	SMOPS
D0	0 to -0.56	0 to -0.81	0 to -0.58	0 to -0.63	0 to -0.57
D1	-0.57 to -0.90	-0.82 to -1.12	-0.59 to -0.84	-0.64 to -1.00	-0.58 to -0.85
D2	-0.91 to -1.18	-1.13 to -1.37	-0.85 to -1.04	-1.01 to -1.23	-0.86 to -1.06
D3	-1.19 to -1.48	-1.38 to -1.67	-1.05 to -1.27	-1.23 to -1.42	-1.07 to -1.29
D4	-1.49 or less	-1.68 or less	-1.27 or less	-1.43 or less	-1.3 or less

841 Table 1(continue). Drought severity information in the original standardized scale.

Categories	WindSat	BDI_s	BDI_w	BDI_b
D0	0 to -0.58	0 to -0.34	0 to -0.31	0 to -0.51
D1	-0.59 to -0.91	-0.35 to -0.56	-0.32 to -0.47	-0.52 to -0.77
D2	-0.92 to -1.18	-0.57 to -0.87	-0.48 to -0.68	-0.78 to -1.00

D3	-1.19 to -1.48	-0.88 to -1.14	-0.69 to -0.87	-1.01 to -1.40
D4	-1.49 or less	-1.15 or less	-0.88 or less	-1.41 or less

842 Table 2 Summary of the commonly used data sets in this paper.

Data	Data Type	Spatial Resolution	Spatial Resolution	Period	Citations
GLDAS Prep	Forcing data	0.25°	3-hourly	2001-2014	Rodell et al., 2004
ESI	Drought Index	0.05°	weekly	2001-2014	Hain et al., 2016
ASCAT	Microwave SM	0.25°	daily	2008-2014	Wagner et al., 1999
WindSat	Microwave SM	0.25°	daily	2008-2014	Li et al., 2010
SMOS	Microwave SM	0.25°	daily	2008-2014	Kerr et al, 2001
SMOPS	Microwave SM	0.25°	daily	2008-2014	Yin et al., 2015b
PDSI	Drought Index	2.5°	monthly	1985-2014	Dai et al., 2013
SPEI	Drought Index	0.5°	monthly	1985-2014	Vicente-Serrano et al., 2010;

843

844

845

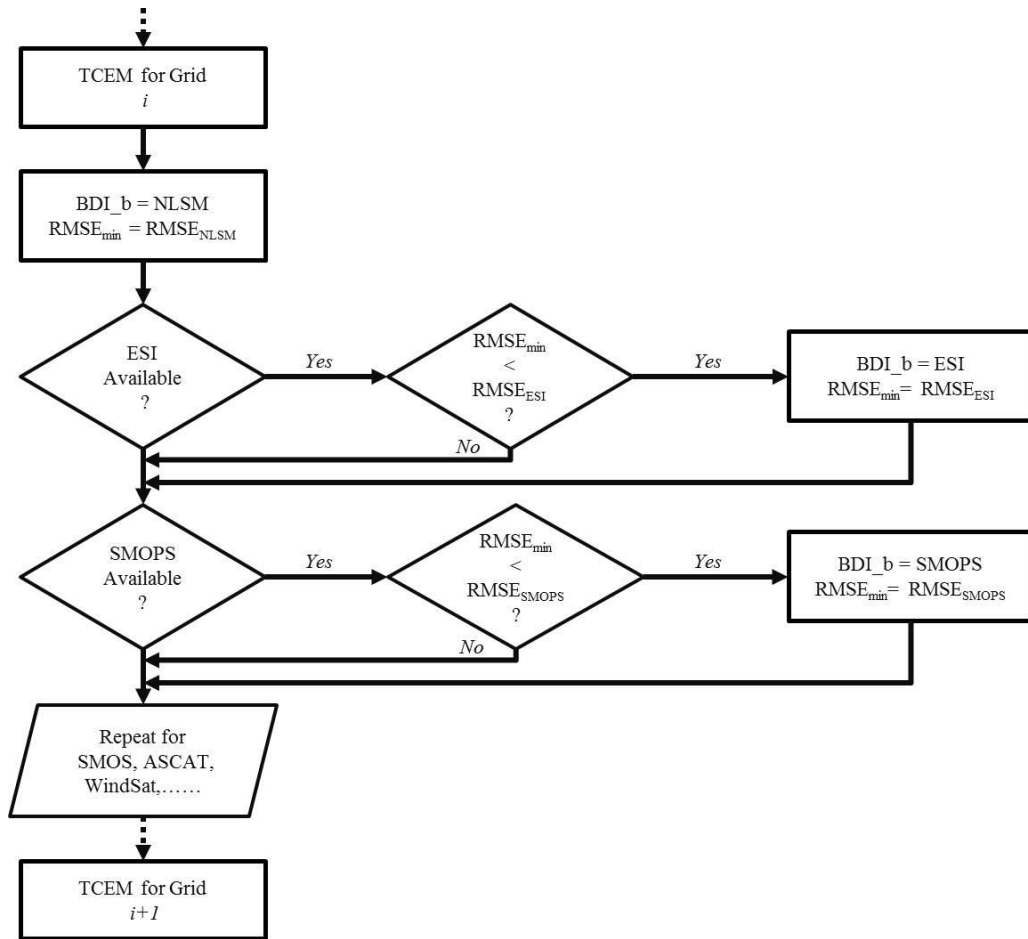


Figure 1 The procedure for constructing the BDI_b using the RMSEs estimated from the Triple Collocation Error Model implemented for each grid in each calendar month. $RMSE_{min}$ is the minimum RMSE for a grid. And $RMSE_{SMOPS}$, $RMSE_{NLSM}$ and $RMSE_{ESI}$ are the monthly RMSE values for soil moisture data sets from SMOPS, NLSM and ESI cases, respectively.

846

847

848

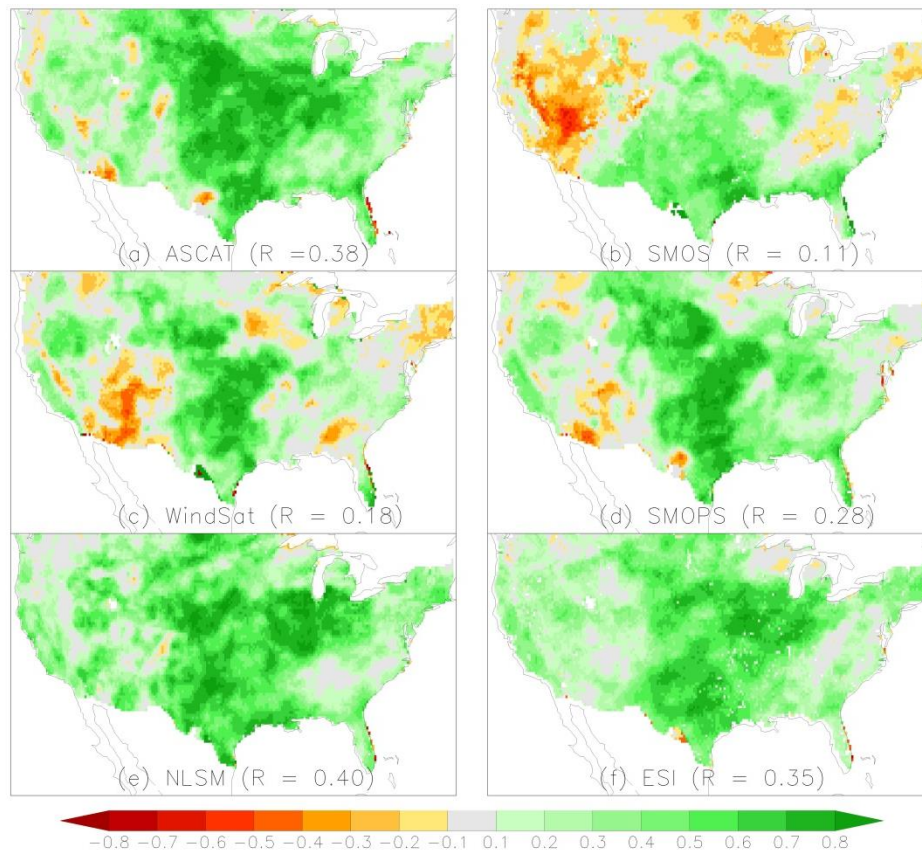


Figure 2 Correlation coefficients (R) between USDM and (a) ASCAT, (b) SMOS, (c) WindSat, (d) SMOPPS, (e) NLSM and (f) ESI. The grey color indicates insignificant correlations.

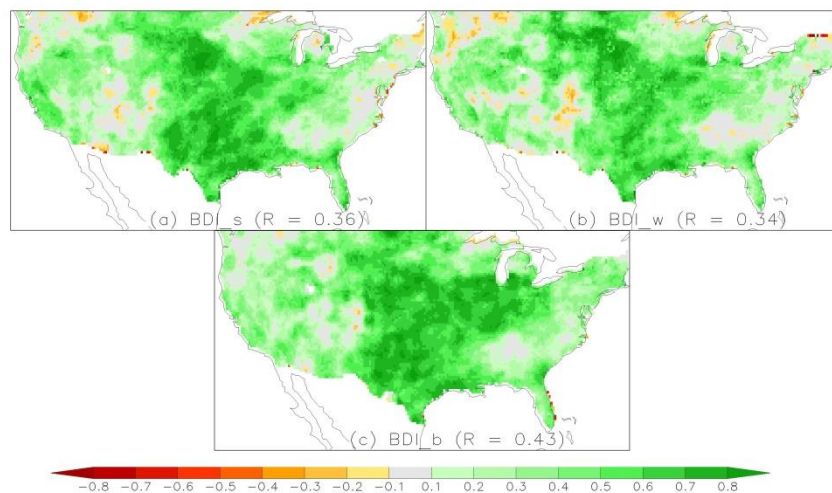


Figure 3 Correlation coefficients (R) between USDM and BDIs over the 2008-2014 period. The grey color indicates insignificant correlations.

849

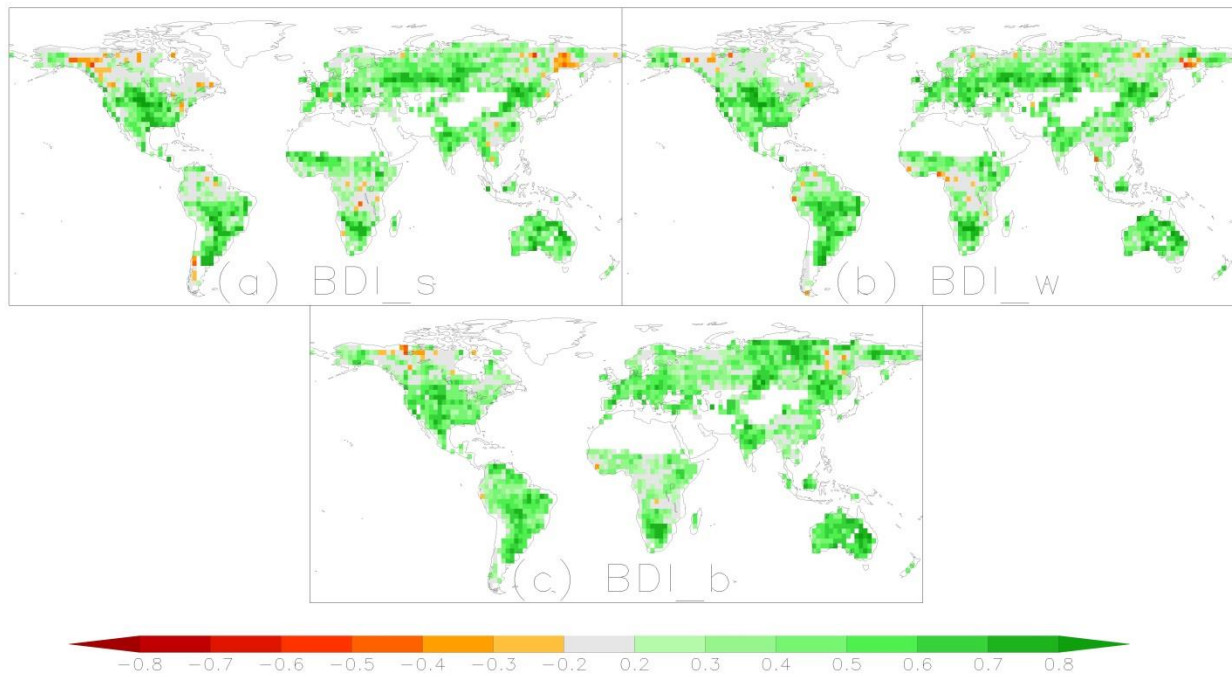


Figure 4 Correlation coefficients between PDSI standard anomalies (against 1985-2014 averages) and BDIs over 2008-2014 period. The grey color indicates insignificance.

850

851

852

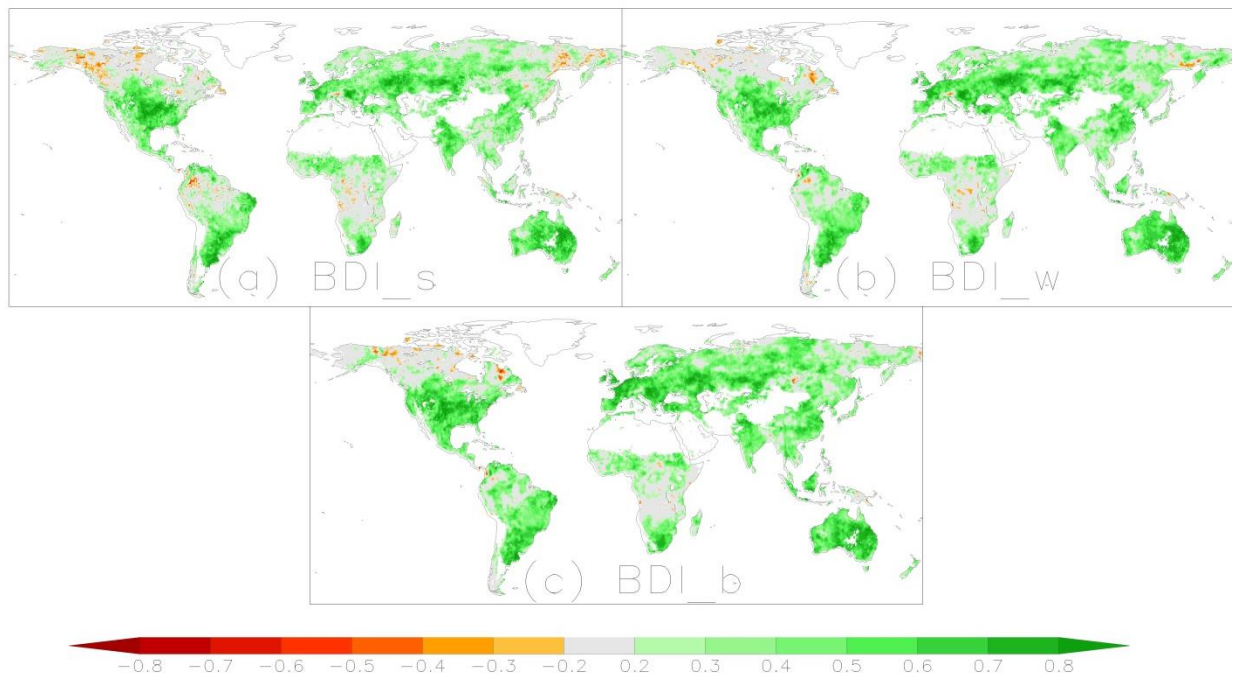


Figure 5 Correlation coefficients between SPEI standard anomalies (against 1985-2014 averages) and BDIs over 2008-2014 period. The grey color indicates insignificance.

853

854

855

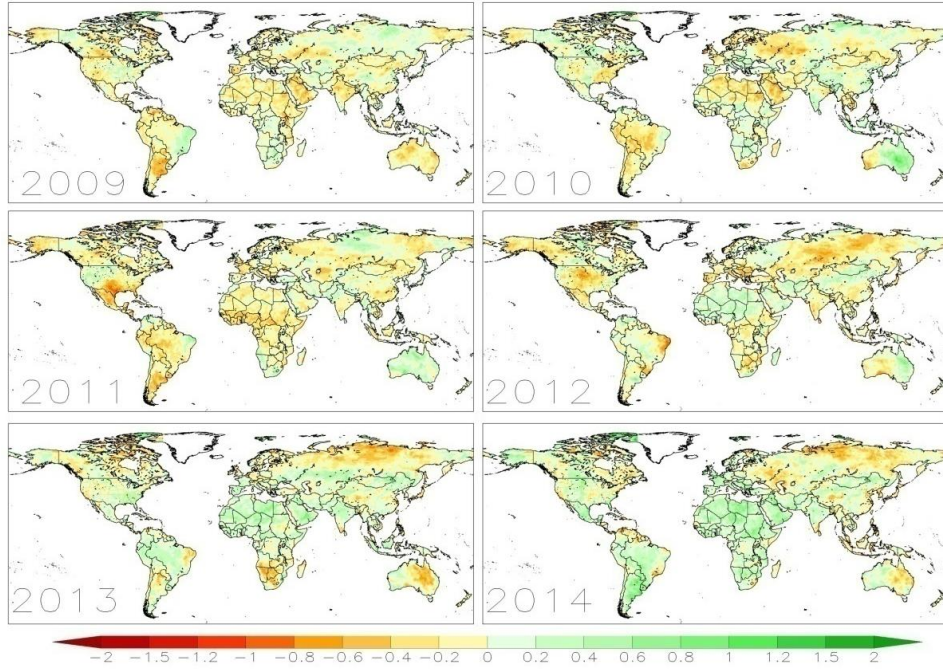


Figure 6(a) Annual global terrestrial BDI_s patterns over the 2009-2014 period. The BDI_s ranges from negative (red) to positive (green) values indicating dry to wet conditions.

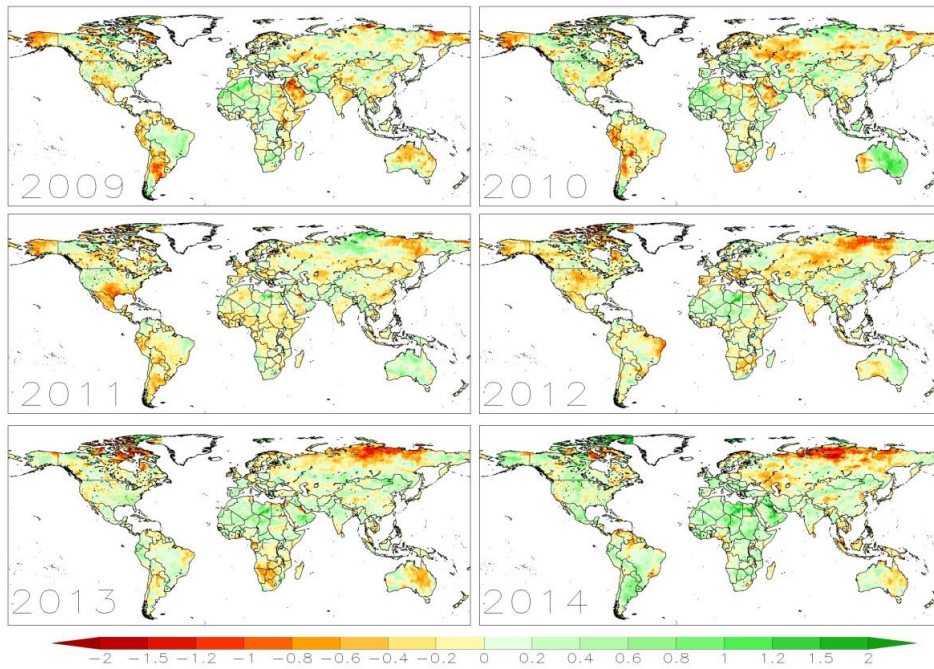


Figure 6(b) Annual global terrestrial BDI_w patterns over the 2009-2014 period. The BDI_w ranges from negative (red) to positive (green) values indicating dry to wet conditions.

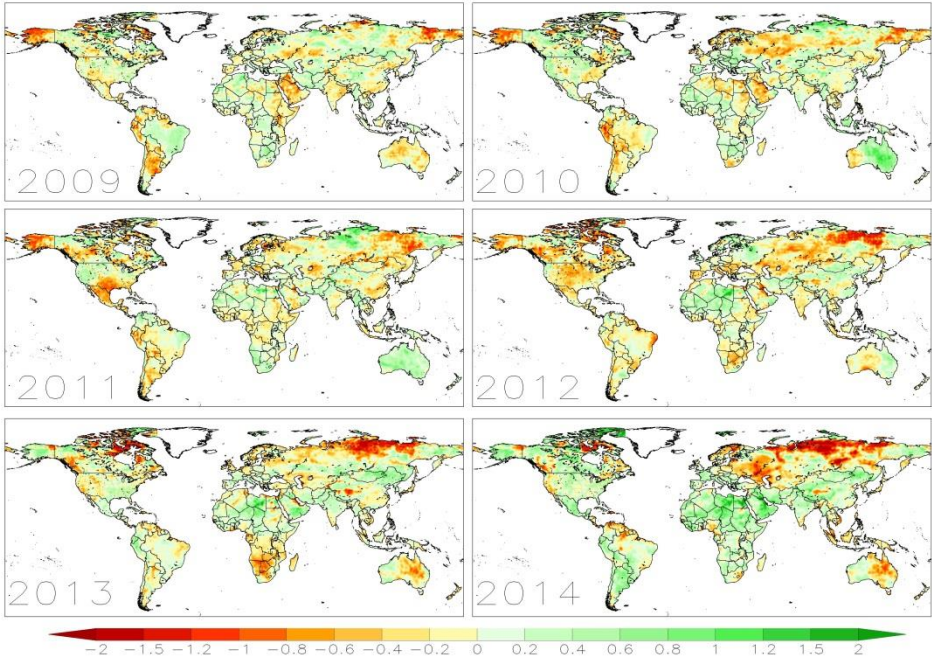


Figure 6(c) Annual global terrestrial BDI_b patterns over the 2009-2014 period. The BDI_b ranges from negative (red) to positive (green) values indicating dry to wet conditions.

856

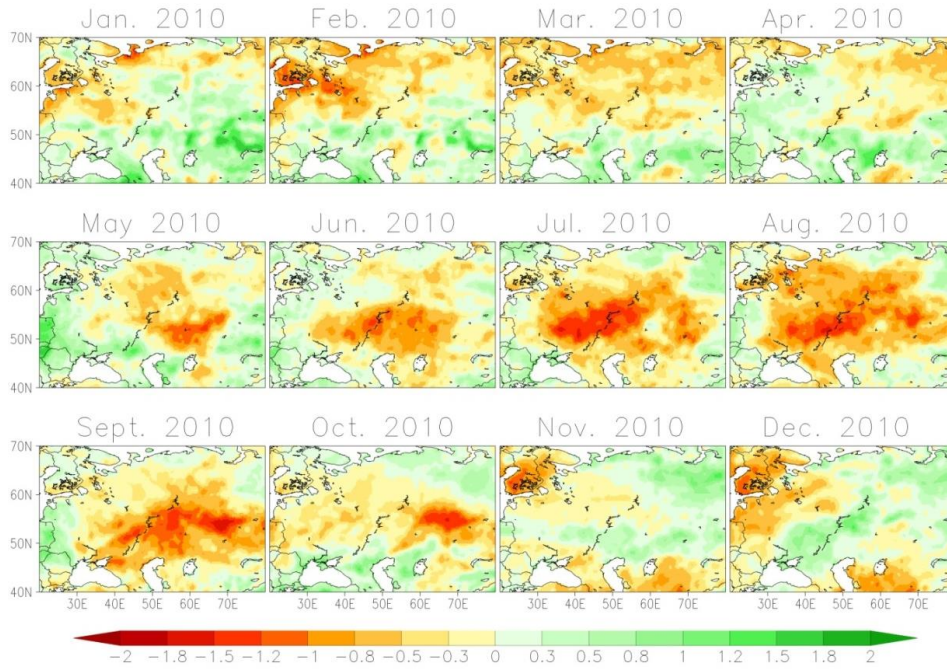


Figure 7(a) Monthly BDI_s on the sub-region (from 40°N, 20°E to 70°N, 80°E) domain in 2010.

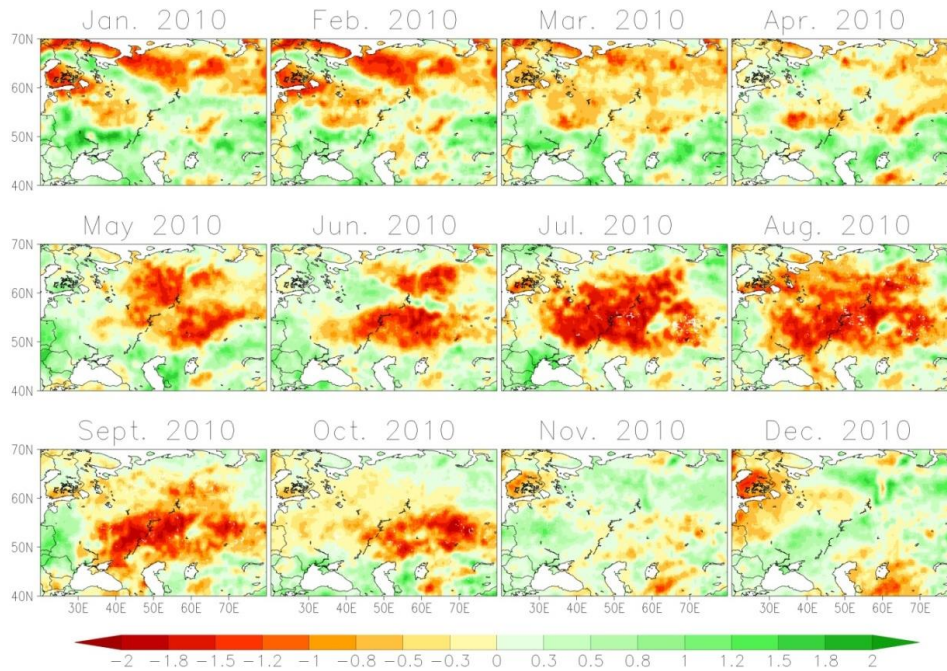


Figure 7(b) Monthly BDI_w on the sub-region (from 40°N, 20°E to 70°N, 80°E) domain in 2010.

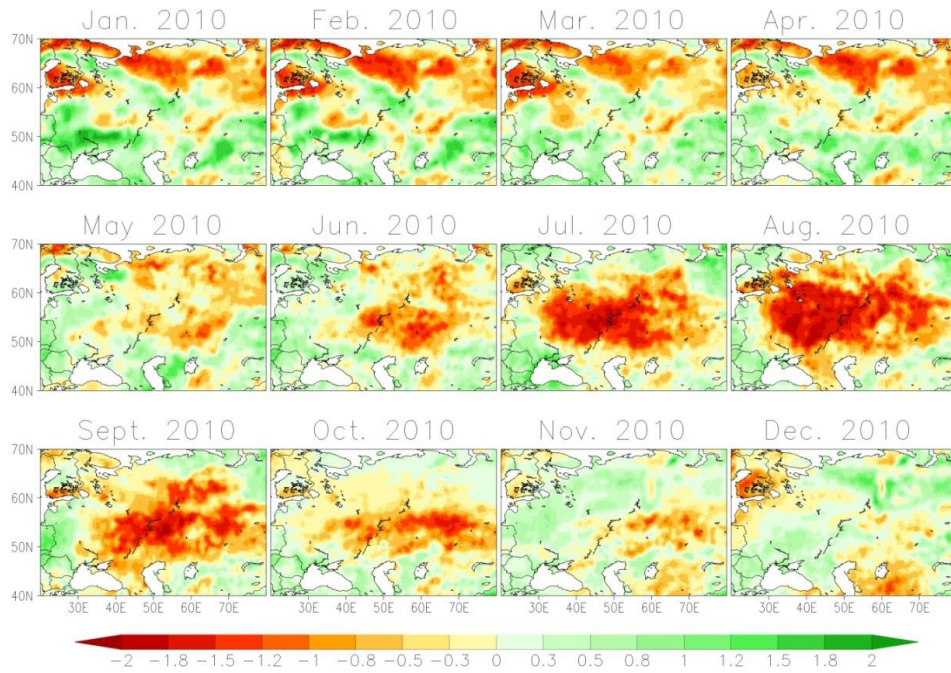


Figure 7(c) Monthly BDI_b on the sub-region (from 40°N, 20°E to 70°N, 80°E) domain in 2010.

857

858

859

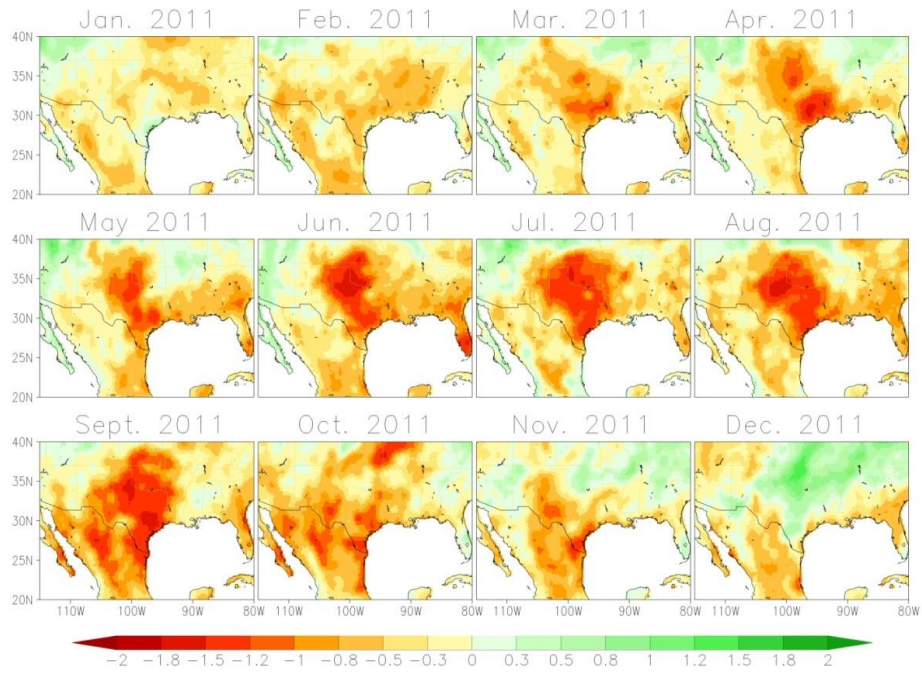


Figure 8(a) Monthly BDI_s on the sub-region (from 25°N, -115°W to 40°N, -90°W) domain in 2011.

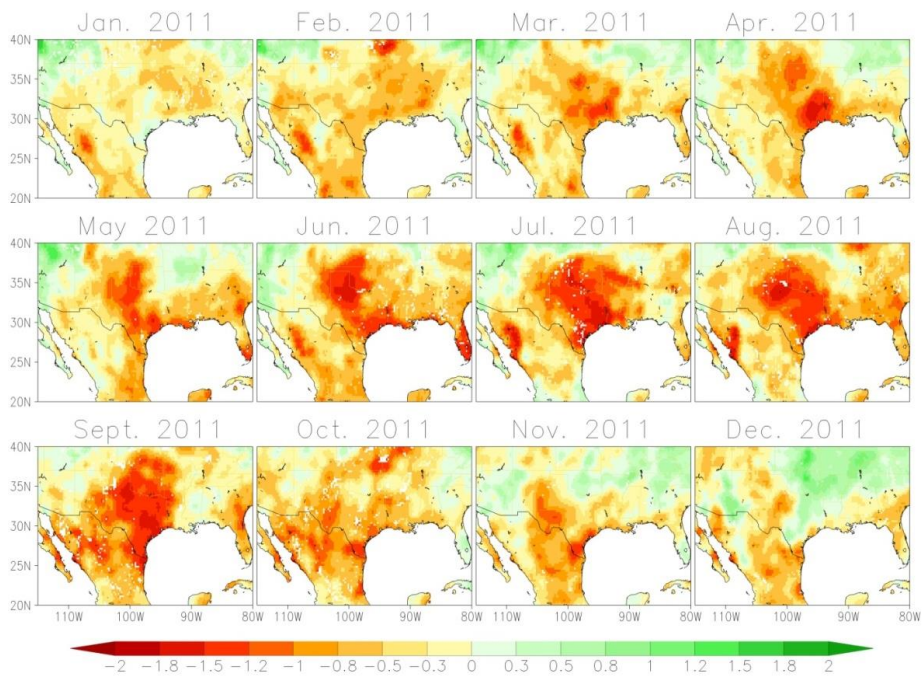


Figure 8(b) Monthly BDI_w on the sub-region (from 25°N, -115°W to 40°N, -90°W) domain in 2011.

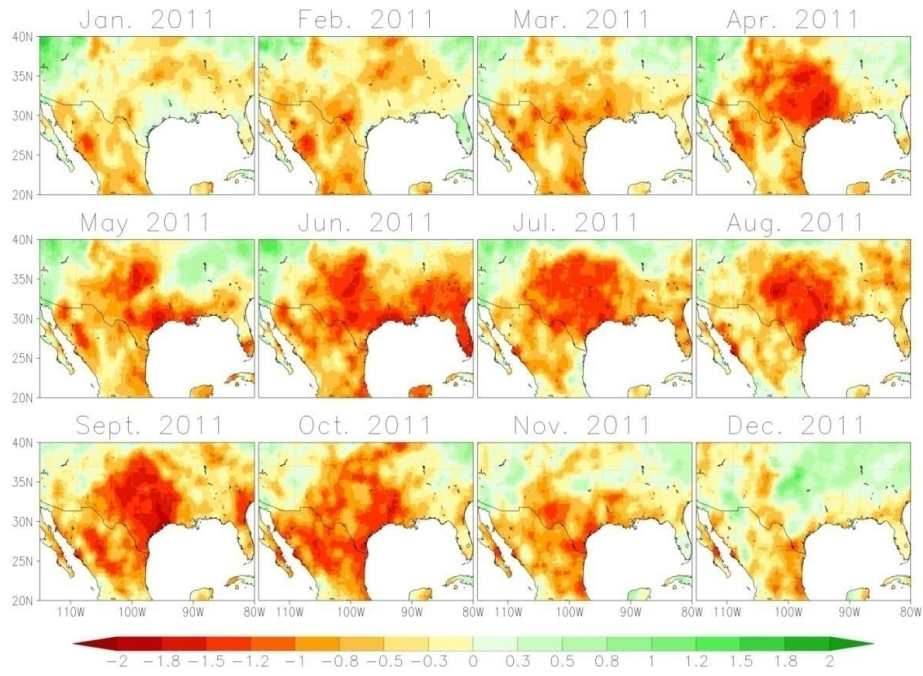


Figure 8(c) Monthly BDI_b on the sub-region (from 25°N, -115°W to 40°N, -90°W) domain in 2011.

860

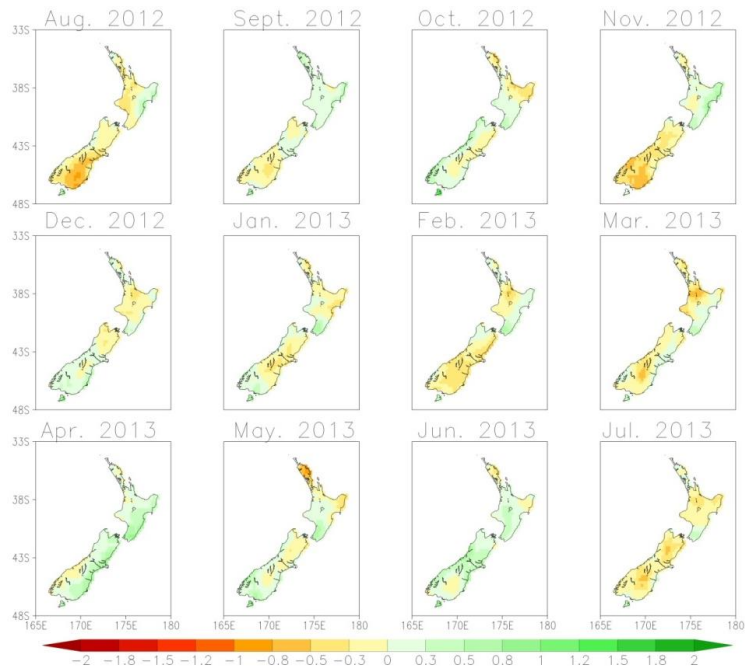


Figure 9(a) Monthly BDI_s across the New Zealand domain (from 48°S, 165°E to -33°S, 180°E) from August 2012 to July 2013.

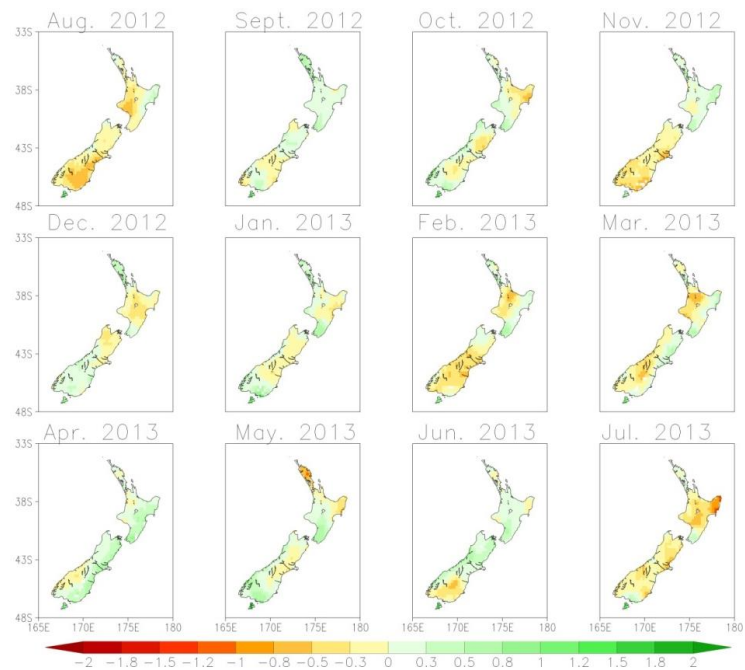


Figure 9(b) Monthly BDI_w across the New Zealand domain (from 48°S, 165°E to -33°S, 180°E) from August 2012 to July 2013.

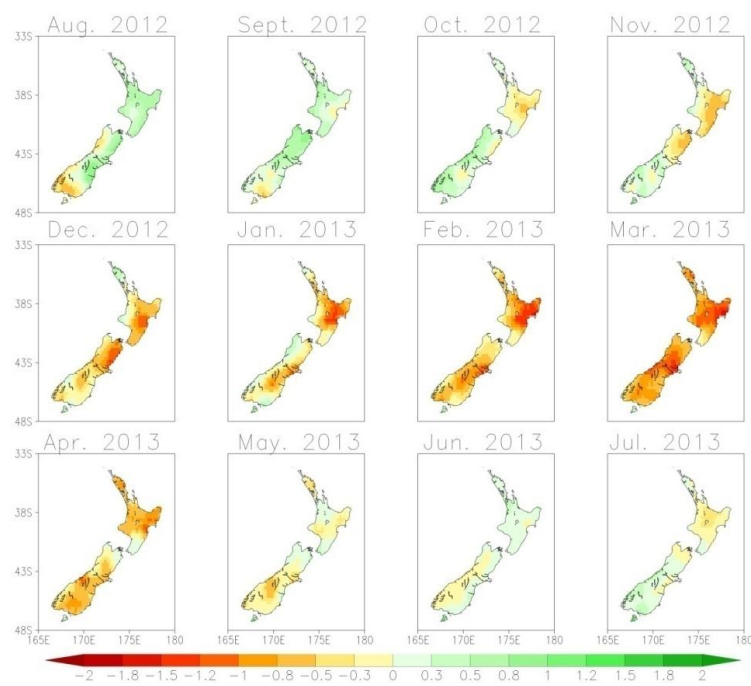


Figure 9(c) Monthly BDI_b across the New Zealand domain (from 48°S, 165°E to -33°S, 180°E) from August 2012 to July 2013.

861